Improvement of the water solubility of tolfenamic acid by new multiple-component crystals produced by mechanochemical methods

UNIVERSITÀ DEGLI STUDI DI TORINO

CRYSTENGCOMM, v. 16 (2014), 8252-8262.

DOI: 10.1039/c4ce00549j

Improvement of the water solubility of tolfenamic acid by new multiple component crystals produced by mechanochemical methods

K. Gaglioti,[a] M. R. Chierotti,[a] F. Grifasi,[a] R. Gobetto,*[a] U. J. Griesser,[b] D. Hasa[c] and D. Voinovich[c]

Received (in XXX, XXX) XthXXXXXXXXX 20XX, Accepted Xth XXXXXXXXX 20XX
DOI: 10.1039/b000000x

Tolfenamic Acid (HTA) is a drug which is characterized by very poor water solubility (13.6 nM in acidic conditions) and moderate solubility in ethanol (0.17 M). A series of new multicomponent crystals have been obtained, by applying mechanochemical methods (i.e. kneading), to mixtures of HTA with sodium acetate, sodium carbonate, sodium hydroxide and imidazole. These reactions resulted in two salts (**NaTA·0.5H_2O** and **NaTA HT Form**), a co-crystal of salts (**NaTA·HTA·0.5NaAc·2H_2O**) and two salt co-crystals (**NaTA·HTA·H_2O/$NaHCO_3$** and **IMH-TA·HTA**). Due to the lack of suitable crystals for single crystal X-ray diffraction analysis, the structural features of the samples have been characterized by solid-state NMR (^{1}H MAS, ^{13}C CPMAS, ^{1}H-^{13}C FSLG LG-CP HETCOR and ^{15}N CPMAS), IR(ATR) and Raman spectroscopies, VT-XRPD and elemental analysis. The evaluation of thermal stability and dissolution behavior was performed using thermogravimetry, differential scanning calorimetry and dissolution kinetic tests. The new solid-state forms show better thermal stability than pure HTA and an improved dissolution rate, which is most pronounced in **NaTA·HTA·H_2O/$NaHCO_3$**, the **NaTA HT Form** and **NaTA·0.5H_2O**.

Introduction

Multicomponent crystal formation (salts and co-crystals) is an effective means with which to tune the properties of a molecule or, in the pharmaceutical field, of an active pharmaceutical ingredient (API) by changing its crystal packing.[1] A co-crystal is a multicomponent molecular crystal; that is, a crystalline substance formed of two or more chemically different molecules.[2] Thus solvates, hydrates and both stoichiometric and non-stoichiometric lattice inclusion compounds are included in this definition.[3] With respect to the pure polymorphism phenomenon, co-crystal formation provides much more in terms of possibilities for modulating crystal packing and this is due to the choice of two parameters: the co-former and the type of weak interaction.[4] The use of inorganic salts as co-formers has already been explored, by our group, as an effective method for producing ionic co-crystals and salt co-crystals of barbituric acid.[5] The difference between ionic co-crystals and salt co-crystals is found in the type of co-former. Ionic co-crystals are formed of an organic molecule and an ionic salt (i.e. alkali halide) in the same asymmetric unit, while salt co-crystals are formed of an organic molecule and one of its salts in the same asymmetric unit.[6]

Tolfenamic acid (HTA, 2-[(2-methyl-3-chlorophenyl) amino] benzoic acid – Scheme 1) is a drug which belongs to the fenamate family. It is a potent, well-tolerated non-steroidal anti-inflammatory drug (NSAID) which displays low gastroulcerogenicity,[7] low overall toxicity and high therapeutic indices as well as analgesic and antipyretic properties.[8] Recent studies have revealed that it is a Cox-2 inhibitor.[9] It is also extensively used in both human and veterinary medicine for its analgesic and antipyretic properties.[10]

A common property of fenamates is their general lack of solubility in water and in other common organic solvents (obviously their solubility is influenced by their polymorphic form)[11] thus HTA belongs to class II of the Biopharmaceutics Classification System (high permeability in cells and low solubility in water).[12]

HTA is known to exist in at least five different polymorphic forms.[13] The most prominent are anhydrous Form I and Form II which show very poor water solubility.[14] In order to improve the water solubility and, thus the biopharmaceutical properties of HTA, we herein report a synthetic strategy for new HTA co-crystal forms which is based on mechanochemical and solution reactions between HTA, inorganic reagents [NaOH, Na_2CO_3 and sodium acetate (NaAc)] and an organic compound such as imidazole (IM). IM is used as a precursor for many pharmaceutical compounds, but is toxic (LD_{50} in pig= 760 mg/kg), and thus not therapeutically used.[15] Nevertheless, we decided to use IM as model co-former in order to study the possibility of an interaction with the COOH group of HTA.

Table 1 Summary of the performed experiments involving HTA and additional components (k = kneading, h= heating).

Components		Preparation	Class	Formula/Name	Ratio
HTA	NaOH	Salification	salt	**NaTA polymorphic mixture**	1:1
NaTA mixture		k (1-BuOH, THF, DMF, H_2O)	salt	**NaTA·0.5 H_2O**	--
HTA	Na_2CO_3	k (EtOH/H_2O 2:1)	heterogeneous mixture with a salt co-crystal	**NaTA·HTA·H_2O/$NaHCO_3$**	2:1
HTA	NaAc	k (EtOH 99%)	co-crystal of salts	**NaTA·HTA·0.5NaAc·2H_2O**	2:1.5
NaTA·0.5H_2O or **NaTA·HTA 2H_2O/$NaHCO_3$**		h (170-180°C)	salt	**NaTA HT form**	
HTA	IM	k (EtOH 99%)	salt	**IMH-TA·HTA**	2:1

Experimental and methods

HTA (Tokyo Chemical Industry Company and Sigma Aldrich), Na_2CO_3, NaOH, IM and NaAc (all Sigma Aldrich) were used without further purification.

The HTA commercial batch was characterized by solid-state NMR analysis as pure Form I. HTA Form II was reproduced following the method reported in literature[16] only for comparison.

All samples were obtained via mechanochemical [kneading with mortar and pestle *i.e.* grinding with catalytic amount (from 50 to 150 µl, corresponding to two-six drops) of solvent] and solvent techniques.[17,]2 Experiments performed and products obtained are summarized in Table 1.

The **NaTA polymorphic mixture** was prepared by refluxing 128 mg of HTA and 1 ml of NaOH 0.5 M (stoichiometric ratio 1:1) in 5 ml of absolute EtOH for 3h.

NaTA·0.5H_2O (salt): A white powder of this hemihydrated salt was quantitatively obtained by kneading (H_2O; 50 µl) a NaTA polymorphic mixture at room temperature for 5 minutes. **NaTA·0.5H_2O** was also obtained by directly kneading (H_2O; 100 µl) HTA with NaOH. However, this procedure did not allow for precise stoichiometric control because the hygroscopic nature of NaOH makes correct weighing difficult. [Elem. Anal. Calc. for $C_{14}H_{12}N_1O_{2.5}Cl_1Na_1$: C, 57.45; H, 4.13; N, 4.79; O, 13.67; Cl, 12.11; Na, 7.85 %. Found: C, 57.26; H, 4.29; N, 4.88; O, 13.72; Cl, 12.08; Na, 7.77 %.]

NaTA·HTA·H_2O/$NaHCO_3$: This is a heterogeneous mixture between NaTA·HTA and $NaHCO_3$. It was not possible to determine whether H_2O co-crystallizes with NaTA·HTA or $NaHCO_3$. It occurs as a white powder and was obtained quantitatively by kneading (ethanol/water 2:1; 150 µl) HTA (200 mg) and Na_2CO_3 (40.5 mg), stoichiometric ratio 2:1, at room temperature for 20 minutes. It was not possible to obtain pure NaTA·HTA without $NaHCO_3$ using different starting material ratios either. The stoichiometric formula: NaTA·HTA·H_2O/$NaHCO_3$ was confirmed by solid-state NMR, thermal analysis and elemental analysis. [Elem. Anal. Calc. for $C_{29}H_{28}N_2O_9Cl_2Na_2$: C, 52.34; H, 4.24; N, 4.21; Na, 6.91 %. Found: C, 52.47; H, 4.29; N, 4.08; Na, 6.88 %.]

NaTA·HTA·0.5NaAc ·2H_2O: This co-crystal of salts was obtained as a white powder and in maximal yield by kneading (EtOH 99%, 150 µl) stoichiometric ratios (2:1.5) of HTA (200 mg) and NaAc (90 mg) at room temperature for 20 minutes. Solid-state NMR, thermal analysis and elemental analysis indicated that the formula is NaTA·HTA·0.5NaAc·2H_2O. [Elem. Anal. Calc. for $C_{29}H_{28.5}N_2O_7Cl_2Na_2$: C, 55.96; H, 4.62; N, 4.50; Na, 7.39 %. Found: C, 55.78; H, 4.56; N, 4.69; Na, 7.19 %.]

NaTA HT Form (salt): A white powder was obtained after heating **NaTA·0.5H_2O** or **NaTA·HTA·H_2O/$NaHCO_3$** at 170-180°C in a muffle oven (ramp 5°C/min). [Elem. Anal. Calc. for $C_{14}H_{11}N_1O_2Cl_1Na_1$: C, 59.27; H, 3.91; N, 4.94; O, 11.28; Cl, 12.50; Na, 8.10 %. Found: C, 59.07; H, 4.13; N, 4.70; O, 11.46; Cl, 12.46; Na, 8.18 %.]

IMH-TA·HTA (Salt co-crystal): This product (white powder) was obtained by kneading HTA (200 mg) and IM (26 mg) in a 2:1 ratio for 15 minutes in the presence of absolute EtOH (50µl). [Elem. Anal. Calc. for $C_{31}H_{28}N_4O_4Cl_2$: C, 62.95; H, 4.77; N, 9.47 %. Found: C, 62.87; H, 4.66; N, 9.32 %.]

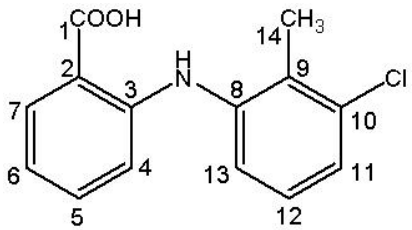

Scheme 1 HTA structure with atom labelling.

All solid-state NMR spectra were recorded with a Bruker Avance II 400 instrument operating at 400.23, 100.65 and 40.55 MHz for ^1H, ^{13}C and ^{15}N nuclei, respectively. For ^{13}C and ^{15}N CPMAS (Cross Polarization Magic Angle Spinning) spectra, cylindrical 4 mm o.d. zirconia rotors with a sample volume of 80 µL were employed. Samples were spun at 12 and 9 kHz for ^{13}C and ^{15}N, respectively. A ramp cross-polarization pulse sequence was used with contact times of 3-5 (^{13}C) or 4 ms (^{15}N), a ^1H 90° pulse of 3.8 µs, recycle delays of 1-60 s and 48-4096 transients for ^{13}C and 1598-5956 transients for ^{15}N. Proton spin–lattice relaxation times, ^1H T_1, were obtained using the ^{13}C-detected Inversion Recovery Cross Polarization technique [^1H(180°-τ-90°)-CP-^{13}C(FID)], where one measures the ^{13}C magnetization that appears through the CP process after the relaxation of ^1H magnetization over time τ. 160-1024 transients were acquired and a variable delay list file (from 22ms to 42s) was used. 2D ^{13}C-^1H FSLG (Frequency Switched Lee Goldburg) on- and off-resonance HETCOR (Heteronuclear Correlation) spectra were measured according to the method developed by van Rossum et al.[18] The

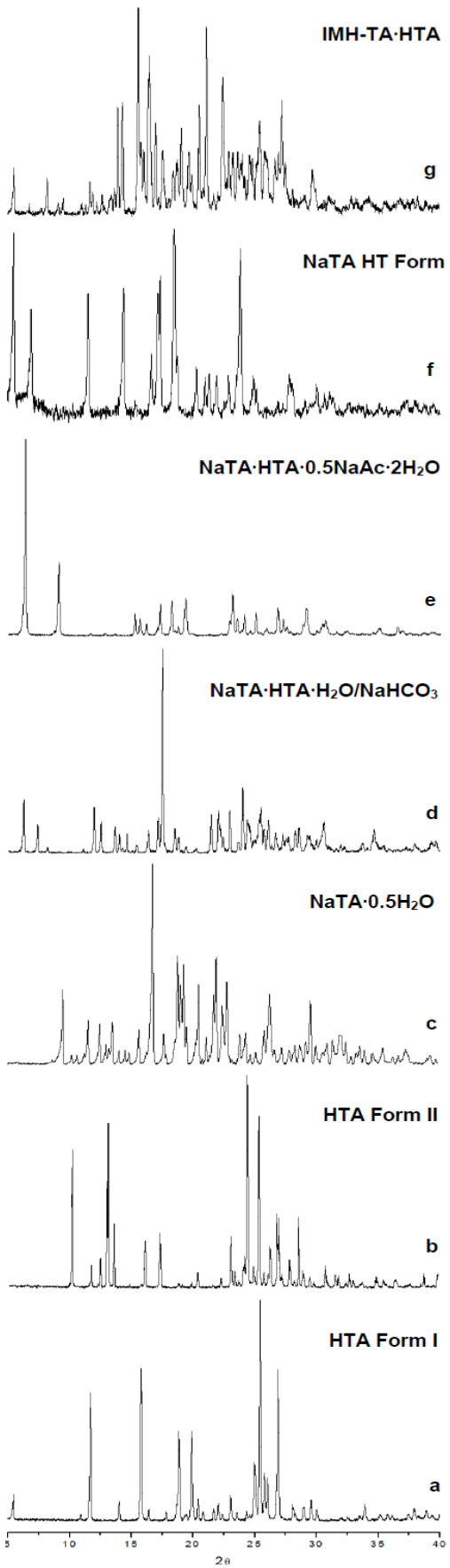

Fig.1 XRPD patterns of HTA and all multiple component crystals.

MAS rate was set at 12 kHz. The proton rf field strength used during the t_1 delay for FSLG decoupling and during the acquisition for TPPM (Two-Pulse Phase-Modulated) decoupling was 83 kHz. Two off-resonance pulses with opposite phases (i.e., +x, -x or +y, -y) used during the FSLG decoupling were set to 9.8 μs. The contact time used was 100 μs. The magic angle (54.7°) pulse length for protons was set at 2.0 μs, while the recycle delay used was 15 s. Quadrature detection was achieved using the States-TPPI method. All data for 64 t_1 increments with 140 scans were collected. A $B_1(^1H)$ field intensity for the CP of 75 kHz and a mixing period of 2.0 ms were used for FSLG off-resonance CP (LG-CP) HETCOR NMR. The ^1H NMR chemical shift scale in the HETCOR spectra was corrected by a scaling factor of $1/\sqrt{3}$ because the ^1H NMR chemical-shift dispersion is scaled by a factor of $1/\sqrt{3}$ during FSLG decoupling. ^1H MAS experiments were performed on a 2.5 mm Bruker probe at a spinning speed of 32 kHz. The ^1H MAS spectra were acquired using the DEPTH sequence ($\pi/2–\pi–\pi$) which suppresses the probe background signal.[19] The ^1H 90° pulse length was set to 2.50 μs, the recycle delays to 1-40 s and 32-64 transients were averaged for all samples. ^1H, ^{13}C and ^{15}N chemical shifts were referenced via the resonance of solid adamantane (^1H signal at 1.87 ppm), HMB (^{13}C methyl signal at 17.4 ppm) and $(NH_4)_2SO_4$ (^{15}N signal at -355.8 ppm with respect to CH_3NO_2), respectively.

IR and Raman spectra were only used to screen the products and to monitor reaction conversion. In order to discriminate between the different forms, particular attention was given to the regions from 3500 to 3300 cm^{-1} (NH and OH stretching), 3100 and 3000 cm^{-1} (CH and CH_2 stretching) and 1700-1600 cm^{-1} (C=O stretching). All IR and Raman spectra are reported in Figures S1 and S2 in the Supporting Information. Fourier transform infrared (FTIR) spectra were collected directly on the sample using a Bruker IFS 25 spectrometer (BrukerAnalytischeMesstechnik GmbH, Ettlingen, Germany) connected to a Bruker IR microscope I (15x-Cassegrain-objective). The samples were prepared on ZnSe-disks and measured in transmission mode (spectral range 4000-600 cm^{-1}, resolution 4 cm^{-1}, 32 interferograms per spectrum).[20] Raman spectra were measured on a Bruker Vertex 70 spectrometer equipped with a RAM II using a 1064 nm Nd:YAG source and a Ge diode detector (laser power 10-50 mW, spectral resolution 4 cm^{-1}).

Differential Scanning Calorimetry (DSC) was performed on a TA instrument Q200. Samples (5-10 mg) were placed in sealed alumina pans and heated at a rate of 10°C min^{-1} (temperature range: 30 to 400 °C).

Thermogravimetric (TGA) measurements were performed under N_2 flow (heating rate: 10°Cmin^{-1}) on a TA instrument Q600 SDT Simultaneous DSC-TGA heat flow analyzer. The samples (5-10 mg) were placed in alumina pans. All DSC and TGA thermograms are reported in Figures S3 in the Supporting Information.

X-ray powder diffraction (XRPD) patterns of the samples under investigation were collected on a PW3050/60 X'Pert PRO MPD diffractometer, from PANalytical, working in the Debye-Scherrer geometry and using, as the source, a high-powered ceramic tube PW3373/10 LFF with a Cu anode equipped with a Ni filter to attenuate Kb which was focused by a PW3152/63 -

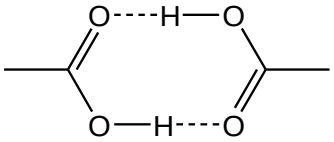

Scheme 2 Supramolecular Synthons and Hydrogen Bond motif of anhydrous HTA Form I and II.

X ray mirror. Powdered samples were hosted inside a 0.8-mm boron silicate capillary and mounted on a rotating goniometer head.

Variable Temperature (VT) XRPD studies were carried out on an X-Pert Diffractometer (PANalytical, Cu Kα radiation) equipped with a hot-stage and an environmental chamber (Anton Paar XRK 900), to analyze the conversion of both **NaTA·0.5H$_2$O** and **NaTA·HTA·H$_2$O/NaHCO$_3$** to the **NaTA HT Form**. XRPD patterns of HTA Form I, Form II, and all multiple component crystals are reported in Figure 1, while XRPD patterns of used co-formers, VT-XRPD patterns, used ramps and technical details are reported in the Supporting Information (Figures S4 and in Schemes 1 and 2).

Dissolution kinetic tests (DKT) were performed in a pH 7.4 buffer (0.2 M KH_2PO_4/0.2 M NaOH). 5 mg of HTA (as a pure compound or co-crystal and salt) were added to 150 cm^3 of dissolution medium at 37°C in each experiment. The release test lasted 180 min. In these experiments, the solution was kept homogeneous using an impeller (rotational speed 200 rpm) and the determination of HTA concentration was performed using fibreoptic apparatus (HELLMA, Milano, Italy) connected to a spectrophotometer (ZEISS, Germany,).[21] Measurement was performed at 286.9 nm (HTA maximum absorption, supporting information). Each sample was tested in triplicate. The mother solution was obtained by dissolving 100 mg HTA in 100 ml methanol. The concentration of the standard solutions obtained from the mother solution and the calibration curve are reported in Figures S5 in the Supporting Information. In this dissolution medium, the equilibrium solubility of pure HTA was 28.5 mg/l.
Elemental analysis was performed on a CHN analyzer (CE Instruments, NA2100 Protein), and a Perkin Elmer 3030 flame atomic absorption spectrometer (FAAS) for sodium determination, to clarify the stoichiometry of compounds. The data confirm the stoichiometries deducted by solid-state NMR. Data are reported in the Experimental and methods section.

Results and discussion

The two anhydrous forms of HTA are characterized by the presence of a dimer which is connected through the very robust $R_2^2(8)$ carboxylic acid homo-dimeric synthon (Scheme 2), as observed in the X-ray structures.[22] Such a feature gives rise to a single COOH resonance around 175 ppm in the ^{13}C CPMAS spectra (Figure 2a and 2b). This is an intermediate value between typical COOH and COO$^-$ chemical shifts (~173 and ~178 ppm, respectively).[23] The strength of this interaction most likely explains the poor water solubility of HTA. Although one example of a HTA co-crystal,[24] five metal-complexes[25] and a calcium salt are reported in literature,[26] the $R_2^2(8)$ carboxylic acid homo-dimeric synthon is strong enough to prevent the formation of other co-crystals in which the COOH group must be accessible.
Indeed, the NH group is not particularly suitable for hydrogen bond interaction as both the steric hindrance of the methyl and COOH groups and the formation of an intramolecular hydrogen bond with the COOH moiety hamper it. This is probably the main reason why it does not form classic organic co-crystals with malonic acid, succinic acid, sodium malonate, glycine, L-alanine, aspartic acid, sodium glycinate, sodium acetate (NaAc), adenine, thymine, guanine and resorcinol. The ionic co-crystal approach,[27] using inorganic salts (KI, KF, KBr, NaCl, KBr, $KHCO_3$, K_2CO_3, $NaHCO_3$, $AlCl_3$ e $FeCl_3$,) was also unsuccessful. For this reason we decided to use co-formers which are either able to react quantitatively with HTA, to form the corresponding salt, or to partially salify HTA and form a salt co-crystal such as salts and bases: NaOH, Na_2CO_3, NaAc and IM.

All samples were obtained via simple kneading. Crystallization with different solvents resulted in either a NaTA polymorphic mixture or pure HTA Form I or II. Different forms are present in the NaTA polymorphic mixture, as shown by the ^{13}C CPMAS spectrum (Figure S6 in the Supporting Information). Several attempts to promote the selective crystallization of single forms using various solvents (EtOH, 1- BuOH, THF, DMSO, DMF, H_2O or CH_3CN) failed. Thus, in this case, mechanochemistry allowed us to obtain pure compounds. The chemical shifts of the solid-state NMR spectra of all crystal forms are listed, with assignments, in Table 2.

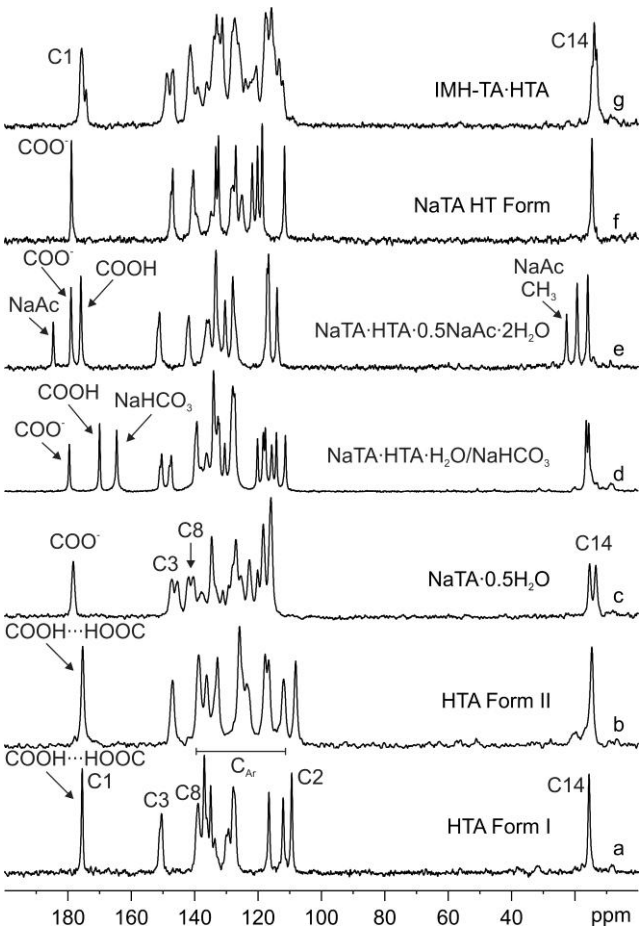

Fig. 2 ^{13}C (100 MHz) CPMAS spectra with main the assignments of HTA Form I and II, **NaTA·0.5H$_2$O**, **NaTA·HTA·H$_2$O/NaHCO$_3$**, **NaTA·HTA·0.5NaAc·2H$_2$O**, **NaTA HT Form** and **IMH·TA·HTA** recorded at 12 kHz.

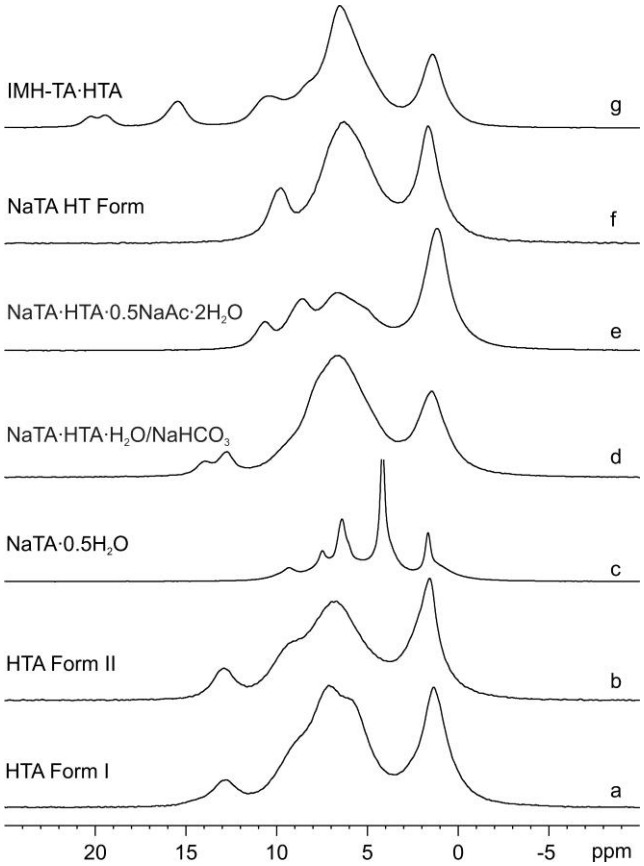

Fig. 3 ^{1}H (400 MHz) MAS spectra of HTA Form I and II, **NaTA·0.5H$_2$O**, **NaTA·HTA·H$_2$O/NaHCO$_3$**, **NaTA·HTA·0.5NaAc·2H$_2$O**, **NaTA HT Form** and **IMH-TA·HTA** recorded at 32 kHz.

NaTA·0.5H$_2$O, prepared in a pure form by kneading stoichiometric amounts of HTA and NaOH, shows the splitting of almost all resonances in the ^{13}C CPMAS spectrum (Figure 2c), indicating the presence of two independent molecules in the unit cell. The splitting is especially marked for atoms C3, C8 and C14. Salification was confirmed by the shift of the carboxylic resonance from 175.3 ppm (typical of the cyclic dimerization of the COOH moieties in pure HTA) to 178.3 ppm, which is characteristic of the COO$^-$ group. The possible formation of a 50:50 mixture between two polymorphs was ruled out by ^{1}H T_1 measurements which provided the same value for all ^{1}H atoms. Indeed, according to a simplified but reliable approach,[28] the spin diffusion process averages ^{1}H T_1 when protons belong to the same phase or in the case of homogeneous samples on a nanometer scale.[29] On the other hand, protons with different relaxation times belong to different domains with an average linear dimension of greater than about 100 Å and *vice versa*.[30] In this case all resonances possess the same T_1 values, thus, two molecules are present in the asymmetric unit. The presence of half a water molecule in the structure has been predicted by combining data from TGA (see Figures S3 in the Supporting Information) and integral values of the ^{1}H MAS spectrum (Figure 3c). This value agrees with the elemental analysis. The NH proton chemical shift suggests the presence of the NH···COO$^-$ intramolecular interaction that characterizes both HTA Form I and II and all the crystal forms presented in this paper.

NaTA·HTA·H$_2$O/NaHCO$_3$ was obtained by kneading HTA and Na_2CO_3 (2:1) with an EtOH/H_2O (2:1) mixture used as the mediating solvent. This heterogeneous mixture consists of a salt co-crystal (concomitant presence of both neutral HTA molecule and NaTA salt; NaTA·HTA) and an inorganic salt ($NaHCO_3$) in a different domain. Any other attempt to change either the stoichiometric ratio or grinding conditions yielded a heterogeneous mixture of components. The ^{13}C CPMAS spectrum (Figure 2d) shows two sets of signals which indicate the presence of a HTA and a NaTA molecule in the unit cell. The carboxylic region of the spectrum is characterized by three peaks at 179.3, 170.1 and 164.5 ppm. The two former signals are attributed to the COO$^-$ (179.3 ppm, NaTA) and COOH (170.1 ppm, HTA) groups. The latter peak (at 164.5 ppm) is assigned to the bicarbonate formed during the reaction. Interestingly, ^{1}H T_1 measurements indicate that HTA and TA$^-$ signals belong to the same phase, which is in agreement with the formation of a salt co-crystal, while the $NaHCO_3$ resonance belongs to a different domain.[30] The ^{1}H MAS spectrum (Figure 3d) is characterized by two signals in the hydrogen bond region (14.0 and 12.8 ppm, integral ratio 1:2) which are attributed to the COOH of HTA and NH of HTA and TA$^-$. TGA and ^{1}H integral values suggest the presence of one molecule of H_2O which is in agreement with the elemental analysis. However, it was not possible to establish whether the water is associated with the salt co-crystal or $NaHCO_3$.

NaTA·HTA·0.5NaAc·2H$_2$O was obtained as a pure compound via kneading (EtOH 99%) HTA with NaAc. The carboxylic/carboxylate region of the ^{13}C solid-state NMR spectrum (Figure 2e) reveals the number of independent molecules in the unit cell and revealed the presence of one HTA (δ_{COOH}= 175.9 ppm), one NaTA (δ_{COO-}= 179.0 ppm) and one NaAc (δ_{COO-}= 184.7 ppm) in a 1:1:0.5 ratio. The signals due to the NaAc are only slightly shifted from the pure compound values, indicating a weak interaction with NaTA·HTA (184.7 and 22.8 ppm in **NaTA·HTA·0.5NaAc·2H$_2$O** with respect to 183.5 and 26.7 ppm in pure NaAc). The ^{1}H MAS spectrum (Figure 3e) shows two resonances in the weak hydrogen bond region at 10.8 and 8.6 ppm (ratio 2:1), which are assigned to COOH and NH proton and to the other NH proton (overlapped with aromatic resonances), respectively. By evaluating the ^{1}H integration, we can assume the presence of two molecules of water in the structure, as confirmed by TGA and elemental analysis. The final composition is: NaTA·HTA·0.5NaAc·2H_2O. The same ^{1}H-T_1 value for all the protons confirms that the best definition for describing such structure is a co-crystal of salts (**NaTA·HTA·0.5NaAc·2H$_2$O**), because the solid is composed of a salt co-crystal (NaTA·HTA) and a salt (NaAc). ^{1}H-^{13}C FSLG on- and off-resonance CP HETCOR experiments were performed in order to obtain a deeper understanding of the spatial proximities and to complete the assignment of the strongly overlapped ^{1}H resonances. The spectra are reported in Figures S7 (Supporting Information) and Figure 4, respectively. These experiments allow intra- and intermolecular heteronuclear correlations to be obtained.[31,18] By acquiring 2D experiments with short or long contact times (100 and 2000 μs, respectively), it is possible to discriminate between short- (single bond) and long-range spatial proximities, respectively. In particular, the use of off-resonance CP (LG-CP) allows for a more detailed analysis

Table 2 ^{1}H, ^{13}C and ^{15}N chemical shifts with assignments for all obtained compounds and pure IM and HTA Form I and II.

Note	HTA Form I	HTA Form II	NaTA ·0.5 H_2O	NaTA·HTA ·H_2O/$NaHCO_3$	NaTA·HTA·0.5 NaAc·2H_2O	NaTA HT Form	IMH-TA·HTA	IM
				^{13}C CPMAS				
C1	175.4	175.5	178.3	179.3	179.0	178.9	175.7	--
				170.1	175.9		174.3	
C2	109.4	108.2	118.4	114.2	114.0	111.7	113.4	--
				111.4			112.2	
CH_{Ar}/CH_{IM}	136.2	132.8sh	134.6	136.3	133.3	133.4	133.9	137.0
	135.0	125.0	127.0	132.5	128.0	132.5	133.1	127.3
	130.1	123.6	125.4	130.5	117.1	128.4	131.3	115.7
	129.4	122.9	122.8	120.2	116.7	127.9	127.4	
	127.8	117.8	120.2	117.9		127.1	126.1	
	116.6	116.6		115.7		125.4	117.6	
	112.1	111.9				121.9	115.8	
						120.2		
						118.7		
C9	133.6	125.9	131.3	134.0	130.4	128.4	124.0	--
				127.7		or 127.1	120.6	
C10	137.0	136.3	137.8	139.4;	136.2;	134.7	139.9	--
	136.1			138.2	135.5		136.2	
C3	150.4	146.9	147.3	150.5	151.7sh	147.0	148.8	--
			145.6		151.1		146.9	
C8	138.9	138.7	141.9	147.5	142.4sh	140.5	141.4	--
			140.5		141.9			
C14	15.6	14.6	15.4	16.4	19.3	14.7	14.7	--
			13.4	15.6	16.0		13.9	
							13.2	
C[a]	--	--	--	164.5[b]	184.7[c]	--	--	--
					22.8			
				^{15}N CPMAS				
NH	66.5	--	72.2	66.1	--	64.6	71.7	--
			70.8	60.4			67.6	
							62.5	
							59.1sh	
NH^{+}_{IM}/N_{IM}	--	--	--	--	--	--	153.2[d]	220.5[e]
$\overline{NH}_{IM}$	--	--	--	--	--	--	145.5	149.2
				^{1}H MAS				
COOH	12.8	12.9	--	14.0	10.8	--	15.4	--
				12.8				
NH	8.8sh	8.9sh	9.3	14.0	10.8	9.8	10.4	--
				12.8	8.6sh			
CH_{Ar}/CH_{IM}	7.1	7.0	7.5	6.6	7.5	6.4	8.5	7.2
	6.0	6.7	6.4		6.7		6.5	
CH_3	1.4	1.6	1.7	1.5	1.3	1.7	1.4	--
					1.2			
					0.9			
H_2O	--	--	4.2	6.7	1.3	--	--	2.8
NH^{+}_{IM}	--	--	--	--	--	--	20.2	--
							19.5	
NH_{IM}	--	--	--	--	--	--	15.4	14.7

[a]Carbon atoms of either molecules in other phases or of solvents or of co-former molecules. [b] $NaHCO_3$. [c] NaAc. [d] NH^{+}_{IM}. [e] N_{IM}.

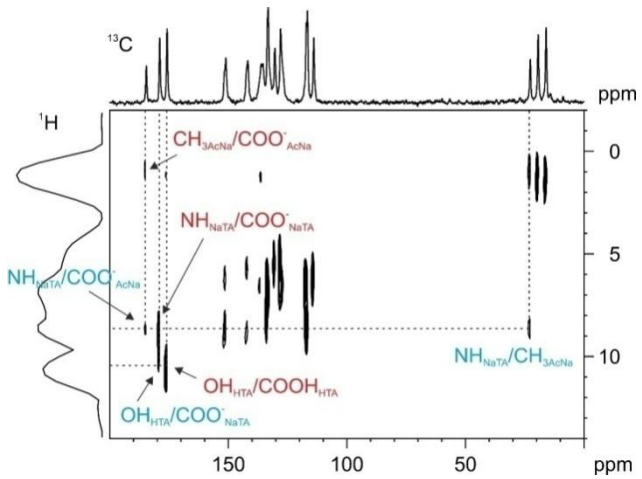

Fig. 4 ^{1}H-^{13}C FSLG LG-CP HETCOR spectrum of **NaTA·HTA·0.5NaAc·2H$_2$O** acquired with a contact time of 2000 µs with relevant assignments. Intramolecular and intermolecular correlations are indicated in red and light blue, respectively.

of long range spatial ^{1}H-^{13}C contacts. This is achieved using a Lee-Goldburg (LG) spin-lock (LG-CP) which efficiently suppresses unwanted ^{1}H–^{1}H spin exchange which leads to fake correlation peaks that reflect ^{1}H-^{1}H homonuclear rather than ^{1}H-^{13}C heteronuclear dipolar couplings.[32,18] All ^{1}H-^{13}C proximities are depicted in Scheme 3. The ^{1}H-^{13}C FSLG LG-CP HETCOR experiment (Figure 4), allowed us to establish the presence of an intramolecular NH···O-C hydrogen bond in the NaTA molecule

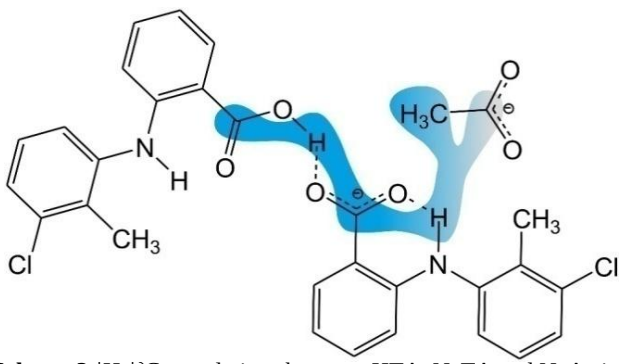

Scheme 3 ^{1}H-^{1}^{3}C correlations between HTA, NaTA and NaAc in **NaTA·HTA·0.5NaAc·2H$_2$O** as deduced from ^{1}H-^{13}C FSLG LG-CP HETCOR.

(correlation between the ^{1}H NH signal at 8.6 ppm and the ^{13}C COO^{-} at 179 ppm). The lack of a similar correlation between signals assigned to the HTA molecule points to a non-planar conformation of the two rings for this molecule. On the other hand, the HTA OH proton (10.8 ppm) correlates with the COO^{-} carbon of NaTA (179.0 ppm), indicating that the two groups are involved in a O-H···O hydrogen bond. Other correlations were found for the NH hydrogen of NaTA (8.6 ppm) with the NaAc methyl and carboxylate carbons (22.8 and 184.7 ppm, respectively). Finally, polarization transfer is observed from the ^{1}H HTA OH (10.8 ppm) to the NaAc methyl (22.8 ppm).

NaTA HT Form - It is possible to obtain an anhydrous high temperature form, called the **NaTA HT Form** which is also stable at room temperature, via heating both **NaTA·0.5H$_2$O** and **NaTA·HTA·H$_2$O/NaHCO$_3$** in a oven at around 180°C. However, heating **NaTA·HTA·0.5NaAc·2H$_2$O** results in a mixture of phases, as observed by ^{13}C CPMAS NMR (see Figure S8 in the Supporting Information). The formation of the new form (**NaTA HT Form**) involves the dehydration of **NaTA·0.5H$_2$O** (release of water and formation of NaTA) and the complete salification of the HTA molecule in **NaTA·HTA·H$_2$O/NaHCO$_3$** after the bicarbonate decomposes to CO_2 and H_2O. A combination of ^{13}C and ^{15}N CPMAS data made it possible to reveal the presence of only one NaTA molecule in the unit cell. The shift to 178.9 ppm in the ^{13}C spectrum (Figure 2f) confirms the presence of COO^{-} groups, while the small NH shift (from 66.5, HTA, to 64.6 ppm, NaTA) indicates a slight rearrangement of the weak intramolecular hydrogen bond which involves the NH. This is in agreement with the ^{1}H MAS spectrum (Figure 3f) where the NH group falls at 9.8 ppm.

The solid-state conversions of **NaTA·0.5H$_2$O** and **NaTA·HTA·H$_2$O/NaHCO$_3$** to **NaTA HT Form** were also followed by VT-XRPD (Figure S4, Schemes 1 and 2). The 5-40° 2θ range was used to evaluate the most significant changes in the patterns. In particular, **NaTA·0.5H$_2$O** is characterized by five principal reflections at 9.58, 12.57, 29.76°, which all disappear at 60°C, and at 15.77 and 19.45°, which vanish at 190°C. The appearance of three principal new reflections at 14.70, 17.63 and 20.51°, at the same temperature, points to the formation of the **NaTA HT Form.** On the other hand, **NaTA·HTA·H$_2$O/NaHCO$_3$** is characterized by reflections at 12.42, 17.38 and 18.34°, plus the signals attributed to $NaHCO_3$ (at 30.43 and 34.39°). Upon increasing the temperature to 190°C, the reflection at 17.38° decreases in intensity while all the others disappear, giving the characteristic signals of the **NaTA HT Form.** The disappearance of the $NaHCO_3$ signals agrees with the salification of HTA by the bicarbonate.

IMH-TA·HTA was obtained by kneading (EtOH 99%) HTA and IM in a 2:1 ratio. Two TA^{-} and two HTA independent molecules are present in the unit cell as shown by the ^{13}C CPMAS spectrum (Figure 2g), which is characterized by the splitting of the C1 (175.7 and 174.3 ppm in 3:1 ratio) and C14 (14.7, 13.9 and 13.2 ppm in 1:2:1 ratio) signals. This is also confirmed by ^{15}N CPMAS (Figure 5) where four peaks, caused by the NH group (71.7, 67.6, 62.6 and 59.1sh ppm), are clearly observable. The number of IM molecules is determined, in this case, by ^{15}N CPMAS because the IM ^{13}C resonances fall under the aromatic CH of the TA^{-}/HTA molecules. The estimated number of independent IM molecules is two (^{15}N δ_{NH}=153.2 and 145.5 ppm). The observed shifts for the IM NH resonances (from 220.5 and 149.2 ppm to 153.2 and 145.5 for N and NH,

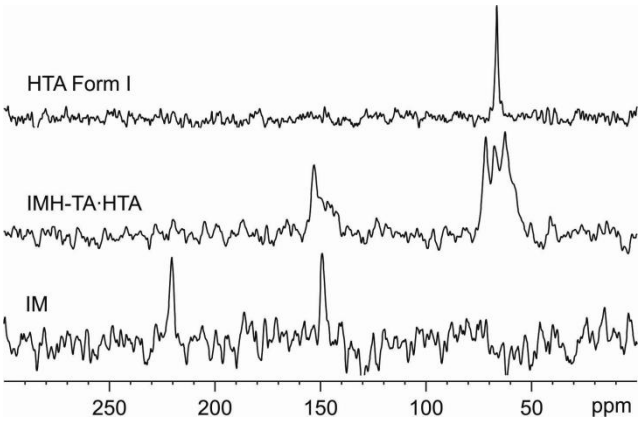

Fig. 5 ^{15}N (40.56 Hz) CPMAS of HTA Form I, **IMH-TA·HTA** and pure IM recorded at 9kHz.

respectively) suggest that the IM is present in the protonated form (imidazolium, IMH^+) as has already been reported in literature.[33] This implies that the proton transfer occurs from one HTA (becoming TA^-) to the IM (becoming IMH^+). The similarity between COOH and COO^- ^{13}C chemical shifts may suggest that an interaction between two groups is able to delocalize the negative charge. It is possible to note, from ^1H MAS (Figure 3g), that the IMH^+ NH^+ groups form very strong hydrogen bonds (20.2 and 19.5 ppm), while the IMH^+ NH and the HTA COOH hydrogen atoms, both involved in hydrogen bonds, fall at the same chemical shift (15.4 ppm). For HTA, as in the ^1H MAS spectra of the other samples, the NH hydrogen is located at 10.4 ppm.

Infrared and Raman Spectroscopy

The Raman and FT-IR spectra of all prepared samples are shown in Figures S1 and S2 in the Supporting Information.

The Raman spectra show clear differences in almost all spectral regions. The most important differences can be found in the COOH/COO^- frequency range (1750-1550 cm^{-1}), reflecting the differences in hydrogen bonding interactions and salt formation. In particular, COOH groups are characterized by ν and δ around 1680 and 890 cm^{-1}, respectively. On the other hand, ν_aCOO^- and ν_sCOO^- are at about 1610 and 1385 cm^{-1}, respectively. Other differences are found in the NH and aromatic CH stretching regions (3500-3050 and 3000-2800 cm^{-1}, respectively). The frequencies of some characteristic bands of the solid-state MIR spectra of the polymorphs and multiple component crystals are listed in Table 3.

Differential Scanning Calorimetry (DSC) and Thermogravimetric (TGA) Analysis

All compounds were investigated using TGA and DSC in order to characterize thermal behavior and to determine the water molecule ratios in the samples. Results are listed in Table 4, while all DSC and TGA figures are displayed in Figure S3 in the Supporting Information.

Heating both **NaTA·0.5H$_2$O** and **NaTA·HTA·H$_2$O/NaHCO$_3$** in an oven at 180°C yielded the same polymorphic form (**NaTA HT Form**). In the case of **NaTA·HTA·0.5NaAc·2H$_2$O**, water release (around 160 °C) is followed by the loss (sublimation) of one HTA molecule (at 182.6°C) that leads to mixtures of anhydrous phases of NaTA and NaAc, as confirmed by ^{13}C CPMAS spectra (see Figure S7 in the Supporting Information).

It is worth noting that the melting and/or decomposition point of all samples, except **IMH-TA·HTA**, are found between 320-339 °C (pure HTA sublimates around 212 °C followed by decomposition) indicating that multicomponent HTA crystals exhibit significantly improved thermal stability over single component forms of HTA.

Table 3 Wavenumbers (cm^{-1}) of characteristic MIR vibrations with assignments for all multiple component crystals and two HTA polymorphs.

	HTA FormI	**HTA FormII**	**NaTA·0.5 H$_2$O**	**NaTA·HTA ·H$_2$O/NaHCO$_3$**	**NaTA·HTA·0.5NaAc·2H$_2$O**	**NaTA HT Form**	**IMH-TA·HTA**
NH	3340,s	3326,s	3343,3255 broad	3279,m	3312,s	3367.5,s3243 .7, broad	3290,s
Ar-CH	3083-2870 w	3078-2914 w	3078-2859 w broad	2676-2388 w broad	3075-2934 w	-	3110-2586 broad
ν(CO)OH	2736-2493 w broad	2733-2487 w	-	-	2740-2591 w	-	-
δ(CO)OH	900,s	886,m	-	-	884,m	-	-
νCO(OH)	1660,s	1668,s	-	1689,s	1775w,1727vs	-	-
$\nu_aCO(O^-)$	-	-	1610,s	1611,s	-	1608.4,s	1579.7,s
$\nu_sCO(O^-)$	-	-	1388,s	1391,1378 broad	-	1379.2,s	1385.4,w
CCl	778,751,m	743,m	756,m	758,m	750,m	752.8,m	752.1,m

Table 4 TGA and DSC data for all achieved samples. T_{H2O}: dehydration temperature, T_{trans}: transition temperature, T_{fus}: melting temperature, T_{dec}: decomposition temperature.

Sample	T_{H2O}	T_{trans}	T_{fus}	T_{dec}
HTA	--	--	210-214	
NaTA·0.5H$_2$O	158.5	67.3, 92.3,191.4[a]	320.9	
NaTA·HTA ·H$_2$O/NaHCO$_3$	--	136.6,160.6[b]	247. 5	339. 1
NaTA·HTA ·0.5NaAc·2H$_2$O	158.0	182.6[c]	334.1	
IMH-TA·HTA	--	109.7	181-213	

[a] solid-solid transitions (*see Supporting Information*). [b]CO_2 and H_2O release due to the HTA salification. [c] release of HTA.

Table 5 Dissolution data: amount (mg/l) of dissolved or released HTA calculated after 1, 15 and 180 minutes with the respective percentage of solubilized sample.

Sample	after 1'	%	after 15'	%	after 180'	%
HTA	0.0	0.0	7.3	21.8	28.5	85.4
NaTA·0.5 H$_2$O	33.0	98.9	33.3	99.8	33.4	100
NaTA·HTA· H$_2$O/NaHCO$_3$	26.1	78.4	32.3	96.8	33.3	100
NaTA·HTA· 0.5NaAc·2H$_2$O	3.7	11.4	19.7	59.1	25.7	77.2
NaTA HT Form	32.1	96.2	33.5	99.8	33.2	99.4
IMH-TA·HTA	0.3	1	5.3	15.8	24.1	72.4

Dissolution kinetic tests (DKT)

In order to confirm that the co-crystallization process is a successful strategy for the improvement of the dissolution properties of HTA, the *in vitro* dissolution performance of pure HTA and various salts and co-crystals were evaluated. Due to its acidic character, the solubility of HTA depends on the pH of the aqueous medium. In fact, it is reported that the solubility of this drug in a pH 1.2 buffer is about 13.6 nM.[34] It is very difficult to detect such extremely low concentrations of HTA using the UV method. Therefore, in the present study a pH 7.4 buffer (where HTA is more soluble) is used as a dissolution medium. The solubility profiles of pure HTA and selected composites are reported in Figure 6 (see Figure S9 in the Supporting information for the complete profile).

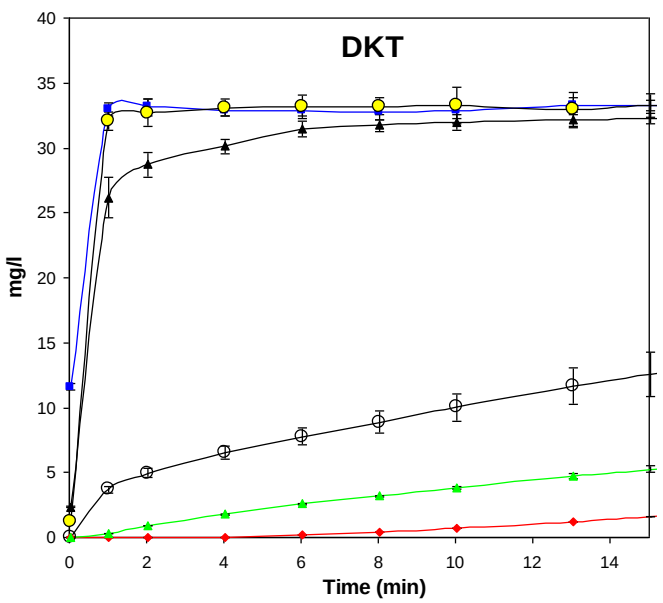

Fig. 6 Dissolution rate profiles of the samples measured in the first 15 minutes: HTA (red line with red circles), **NaTA·0.5H$_2$O** (blue line with blue squares)**, NaTA HT Form** (black line with yellow circles), **IMH-TA·HTA** (green line with green triangles), **NaTA·HTA·H$_2$O/NaHCO$_3$**· (black line with black triangles) and **NaTA·HTA·0.5NaAc·2H$_2$O** (black line with white circles).

Pure HTA shows the typical dissolution profile of a poorly soluble drug: the amount of the drug solubilized remains very low in the first 30 minutes of analysis and increases linearly (due to the protonation phenomenon) in the following part of the dissolution test. Figure 6 shows that the dissolution profile of **IMH-TA·HTA** is very similar to the dissolution profile of pure

Table 6 Concentration C (mg/l), AUC values (mg/l·h) and Frel of all the samples reported for 180, 70 and 15 minutes.

Sample	AUC$_{0-180}$	S.D.	Frel	dFrel
HTA	48.6	3.7	--	--
NaTA·0.5H$_2$O	99.8	2.0	2.1	0.2
NaTA·HTA·H$_2$O/ NaHCO$_3$	98.6	3.0	2.0	0.5
NaTA·HTA·0.5NaAc·2H$_2$O	54.6	13.8	1.1	0.3
NaTA HT Form	99.7	4.0	2.1	0.2
IMH-TA·HTA	42.9	5.2	0.9	0.1

HTA. Better results are obtained by **NaTA·HTA·0.5NaAc·2H$_2$O**, especially in the first part of the analysis (up to 90 minutes), where HTA solubilizes in higher amounts. In the case of **NaTA·0.5H$_2$O** and the **NaTA HT Form**, instantaneous HTA solubilization is observed. In fact, HTA solubilizes completely in the first minute of the dissolution test and high concentrations are maintained throughout. Moreover, no precipitation phenomenon is observed in the dissolution profiles of these forms. It is also worth noting that **NaTA·HTA·H$_2$O/NaHCO$_3$** is completely dissolved in only 15 minutes of analysis, like the NaTA salts (Figure 6). Table 5 lists the data extrapolated after a dissolution time of 1 and 15 minutes. These data highlight how the active component is liberated from the multicomponent samples, and that this process is strongly accelerated not only in the salts but also in **NaTA·HTA·H$_2$O/NaHCO$_3$**.

Subsequently, FDA bioequivalence limits were adopted and used for the *in vitro* solubilization experiments in order to make a comparison between the performed samples. In more detail, FDA guidance suggests that two compounds/formulations can be considered bioequivalent if the ratio of their Area Under the Curve (AUC) is in the 0.80-1.25 interval.[35] This evaluation parameter is proposed for *in vivo* studies, but it has been

successfully applied to compare AUC values obtained from *in vitro* data.[21].

For each sample (pure HTA Form I, HTA salts and HTA co-crystals), AUC was calculated from time 0 to the last measured point (AUC_{0-180}), using the classical trapezoidal method. The AUC of HTA was then used as the reference and indicated as AUC_{ref}. Furthermore, the ratio (indicated as *Frel)* between the AUC of each formulation (AUC_{sample}) and AUC_{ref} was calculated, as follows:

$$Frel = \frac{AUC_{sample}}{AUC_{ref}} \quad \text{(I)}$$

The associated uncertainty (indicated as *dFrel*) for all *Frel* ratios was calculated using the classic formula for the relative error of a ratio:[36]

$$dFrel = |Frel| \sqrt{\left(dAUC_{sample} / AUC_{sample}\right)^2 + \left(dAUC_{ref} / AUCref\right)^2} \quad \text{(II)}$$

where $dAUC_{sample}$ and $dAUC_{ref}$ indicate the S.D. of the AUC_{sample} and AUC_{ref} values, respectively. The calculated *Frel* ± *dFrel* values are listed in Table 6.

It can be seen from Table 6 that **IMH-TA·HTA** and **NaTA·HTA·0.5NaAc·2H$_2$O** are bioequivalent with pure HTA *in vitro*. The other products are probably more bioavailable than pure HTA (Table 6). These results confirm that co-crystallization is an efficient and innovative technique with which to improve the biopharmaceutical performance of poorly soluble drugs.

Conclusions

Three new multicomponent crystals of tolfenamic acid (**NaTA·HTA·H$_2$O/NaHCO$_3$**, **NaTA·HTA·0.5NaAc·2H$_2$O** and **IMH-TA·HTA)** and two sodium salts (**NaTA·0.5H$_2$O** and **NaTA HT Form**) have been prepared using mechanochemical techniques (see Scheme 4). The stoichiometries of the samples were successfully elucidated using a combination of solid-state NMR and TGA data, due to a lack of single crystal XRD analysis. The results are consistent with elemental analysis data. This study thus highlights the great potential that solid-state NMR techniques possess when analyzing the composition and structural characteristics of complex multi-component crystals,[37] for which it may difficult or impossible to acquire single crystal structure data. Indeed, important structural information (asymmetric unit, salt or co-crystal formation, weak interactions, molecule proximities, hydration degree...) for the samples was provided by 1D and 2D solid-state NMR experiments.

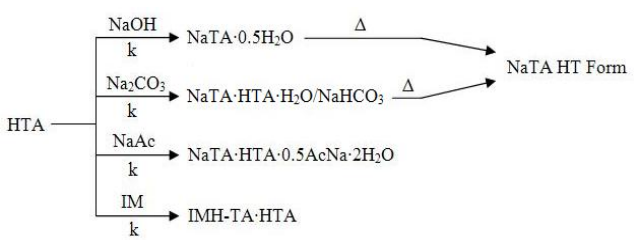

Scheme 4 Representation of the preparation paths. k = kneading, Δ = heating.

Mechanochemistry is a successful method for producing new solid-state forms. One big advantage that this technique provides is the fact that it gives pure products that do not require further purification.

The peculiarities of these HTA derivatives are the following:

- Heating **NaTA·0.5H$_2$O** and **NaTA·HTA·H$_2$O/NaHCO$_3$** results in the same **NaTA HT Form**, as confirmed by solid-state NMR and RAMAN spectroscopy as well as by VT-XRPD measurements. The transformation of the salt hydrate only involves a dehydration process while the transformation of the **NaTA·HTA·H$_2$O/NaHCO$_3$**· to the **NaTA HT Form** includes a salification reaction between the HTA of NaTA·HTA and $NaHCO_3$, which releases CO_2 and H_2O.
- **NaTA·HTA·0.5NaAc·2H$_2$O** behaves differently upon heating and loses HTA to yield a NaTA + NaAc mixture, as characterized by solid-state NMR data.
- All samples show increased thermal stability and improved solubility behavior (especially the **NaTA HT Form**, **NaTA·HTA·H$_2$O/NaHCO$_3$**· and **NaTA·0.5H$_2$O**). All the samples showed this trend for the first ten minutes, while **NaTA·HTA·0.5NaAc·2H$_2$O** and **IMH-TA·HTA** were found to be less soluble than pure HTA, but only after 180 minutes.

This investigation has also demonstrated that the Crystal Engineering approach makes it possible to change, and in these cases improve, the macroscopic properties (dissolution profile and thermal behavior) of an active pharmaceutical ingredient. Dissolution studies confirm that co-crystallization is an efficient and innovative technique with which to improve the biopharmaceutical performance of poorly soluble drugs.

Acknowledgements

We are indebted to Prof. L. Celi for the elemental analyses and Dr. A. Castellero and G. Fiore for the VT XRPD experiments.

Notes and references

1 P. Vishweshwar, J.A. McMahon, J.A. Bis, M.J. Zaworotko, *J. Pharm. Sci.*, **2006**, 95, 499-516
2 T. Friščić, W. Jones, *Cryst. Growth Des.*, **2009**, *9*, 1621–1637
3 J.D. Dunitz, *CrystEngComm*, **2003**, 5, 506-506
4 D. Braga, E. Dichiarante, G. Palladino, F. Grepioni, M.R. Chierotti, R. Gobetto, L. Pellegrino, *CrystEngComm*, **2010**, 12, 3534-3536
5 D. Braga, F. Grepioni, L. Maini, S. Prosperi, R. Gobetto, M.R. Chierotti, *Chem. Commun.*, **2010**, 46, 7715-7717
6 M.R. Chierotti, K. Gaglioti, R. Gobetto, D. Braga, F. Grepioni, L. Maini, *CrystEngComm*, **2013**, 15, 7598-7605
7 O. Eskerod, *Pharmacol. Toxicol.*, **1994**, *75*, 44-48
8 P. A. Insel, in Goodman and Gilman's, *The Pharmacological Basis of Therapeutics*, McGraw-Hill, New York, **1996**, 27
9 a) T. Kawamori, C.V. Rao, K. Seibert, B.S. Reddy, *Cancer Res.*, **1998**, *58*, 409-412; b) H.M. Tucker, R.E. Rydel, S. Wright, S. Estus, *J. Neurochem.*, **1998**, *71*, 506-516
10 S. Cafaggi, E. Russo, G. Caviglioli, B. Parodi, R. Stefani, G. Sillo, R. Leardi, G. Bignardi, *Eur .J. Pharm. Sci*, **2008**, 35, 19-29
11 a) S. Romero, B. Escalera, P. Bustamante, *Int. J. Pharm.*,**1999**, 178, 193-202; b) X.M. Chen, T.L. Li, K.R. Morris, S.R. Byrn, *Mol. Cryst. Liq. Cryst.*, **2002**, 381, 121-131
12 H. Istanbullu, S. Ahmed, M.A. Sheraz, I. urRehman, *BioMed. Res. Int.*, **2013**, 2013, 1-8

[13] V. López-Mejías, J.W. Kampf, A.J. Matzger, *J. Am. Chem. Soc.* **2009**, 131, 4554–4555
[14] a) A. Mattei, T. Li, *Int. J. Pharm*, **2011**, 418, 179-186; b) A. Mattei, T. Li, *Pharm. Res.*, **2012**, 29, 460-470
[15] P.H. Stahl, C.G. Wermuth, *Handbook of Pharmaceutical salts: properties, selection and use*, Ed. Wiley-VCH, Freiburg im Breisgau, **2008**,19-40
[16] R.K. Gilpin, W. Zhou, .*J Pharmaceut. Biomed*., **2005**, 37, 509-515
[17] a) D. Cinčić, T. Friščić, W. Jones, *J. Am. Chem. Soc.*, **2008**, 130, 7524-7525; b) T. Friščić, *Chem. Soc. Rev.*, **2012,** 41, 3493-3510
[18] B.J. van Rossum, C.P. de Groot, V. Ladizhansky, S. Vega, H.J.M. de Groot, *J. Am. Chem. Soc*. **2000**, 122, 3465-3472
[19] a) O.N. Antzutkin, S.C. Shekar, M.H. Levitt, *J. Magn. Reson. Ser. A*, **1995**, 115, 7-19; b) O.N. Antzutkin, Y.K. Lee, M.H. Levitt, *J. Magn. Reson*., **1998**, 135, 144-155
[20] D.E. Braun, T. Gelbrich, V. Kahlenberg, R. Tessadri, J. Wieser, U.J. Griesser, *J. Pharm. Sci.*, **2009**, 98(6), 2010-2026
[21] a) D. Hasa, D. Voinovich, B. Perissutti, A. Bonifacio, M. Grassi, E. Franceschinis, S. Dall'Acqua, M. Speh, J. Plavec, S. Invernizzi, *J.Pharm.Sci.*,**2011**, 100, 915-932; b) D. Hasa, B. Perissutti, M.R. Chierotti, R. Gobetto, I. Grabnar, A. Bonifacio, S. Dall'Acqua, S. Invernizzi, D. Voinovich, *Int. J. Pharm.*,**2012**, 436, 41-57
[22] K.V. Andersen, S. Larsen, B. Alhede, N. Gelting, *J. Chem. Soc. Perkin Trans. II*,**1989**, 1443-1447
[23] a) M. Sardashti, G.E. Maciel, *J. Phys. Chem.*, **1988**, 92, 4620-4632; b) K.M.N. Burgess, M.N. Kevin, X. Yang, C. M. Leclerc, D. L. Bryce, *J. Phys. Chem. A*, **2013**, 117, 6561-6570
[24] L. Fábián, N. Hamill, K.S. Eccles, *Cryst. Growth Des.*, **2011**, 11, 3522-3528
[25] D. K. Demertzi, D. H. Litina, A. Primikiri, M. Staninska, C. Kotoglou, M.A. Demertzis, *Chem. Biodiv.*, **2009**, 6, 948-960
[26] F. Atassi, S.R. Byrn, *Pharm. Res.*, **2006**, 23, 2405-2412
[27] D. Braga, F. Grepioni, L. Maini, D. Capucci, S. Nanna, J. Wouters, L. Aerts, L. Quéré, *Chem. Commun.*, **2012**, 48, 8219-8221
[28] J. Brus, H. Petrícková, J. Dybal, **2002**, In: N. Muller, P.K. Madhu, (Eds.), *Potential and Limitations of 2D 1H–1H Spin-Exchange CRAMPS Experiments to Characterize Structures of Organic Solids in Current Developments in solid-state NMR Spectroscopy*, Springer-Verlag, Wien, 107-137
[29] I. Ando, T. Asakura, *Solid-state NMR of Polymer*. Elsevier, Amsterdam, **1998** (and references therein)
[30] M. Geppi, G. Mollica, S. Borsacchi, C.A. Veracini, *Appl. Spectr. Rev*., **2008**, 43, 202-302
[31] M.R. Chierotti, L. Ferrero, N. Garino, R. Gobetto, L. Pellegrino, D. Braga, F. Grepioni, L. Maini, *Chem. Eur. J.*, **2010**, 16, 4347-4358, b) M.R. Chierotti, R. Gobetto, L. Pellegrino, L. Milone, P. Venturello, *Cryst. Growth Des.*, **2008**, 8, 1454-1457
[32] a) J. Brus, A. Jegorov, *J. Phys. Chem. A*,**2004**, 108, 3955-3964; b) M.R. Chierotti, R. Gobetto, *CrystEngComm*, **2013**, 15, 8599-8612.
[33] a) R.C. Claramunt, C. Lopez, M.A. Garcia, G.S. Denisov, I. Alkorta, J. Elguero, *New J. Chem.*, **2003**, 27, 742-734; b) S. Li, M. Hong, *J. Am. Chem. Soc.*, **2011**, 133, 1534-1544
[34] C.A.S. Bergström, C.M. Wassvik, K. Johansson, I. Hubatsch, *J. of Med. Chem.*, **2007**, 50, 5858-5862
[35] Food and Drug Administration, Guidance for Industry, Bioavailability and Bioequivalence Studies for Orally Administered Drug Products - General Considerations, **2003**.
[36] J.R. Taylor, An Introduction to Error Analysis: The Study of Uncertainties in Physical Measurements. University Science Books, Sausalito, CA, USA, **1997**, 1-464
[37] a) R.K. Harris, *NMR crystallography*. John Wiley & Sons, Chichester, **2009**; b) R.K. Harris, *Analyst*, **2006**, 131, 351-373; c) E. Benedicte, L.Emsley, *J. Am. Chem. Soc.*, **2005**, 127, 9140-9146

Supporting Information

Improvement of the water solubility of tolfenamic acid by new multiple component crystals produced by mechanochemical methods

K. Gaglioti, M. R. Chierotti, F. Grifasi, R. Gobetto,* U. J. Griesser, D. Hasa, D. Voinovich

Figures S1: Raman spectra of all prepared compounds.

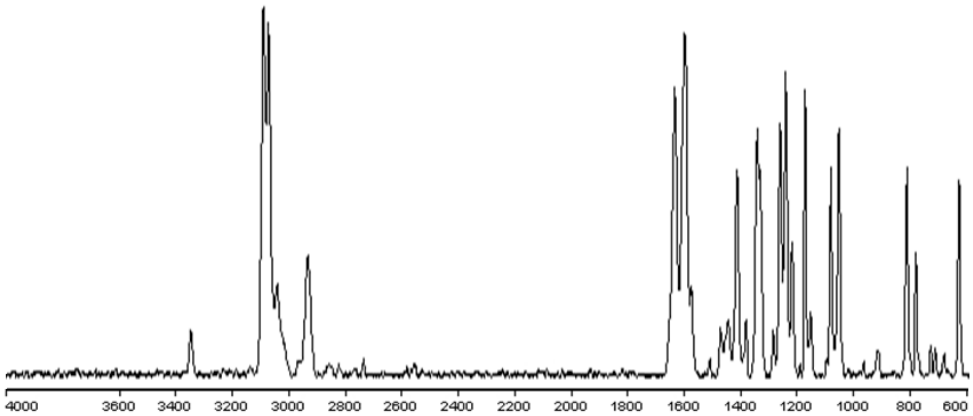

a) Raman spectrum of HTA Form I.

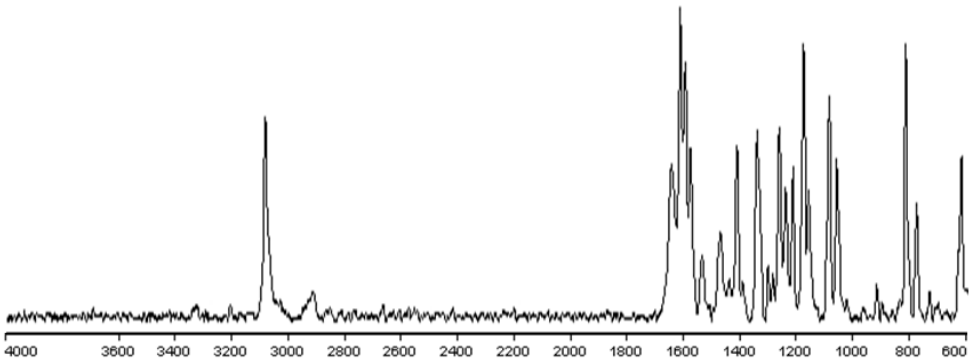

b) Raman spectrum of HTA Form II.

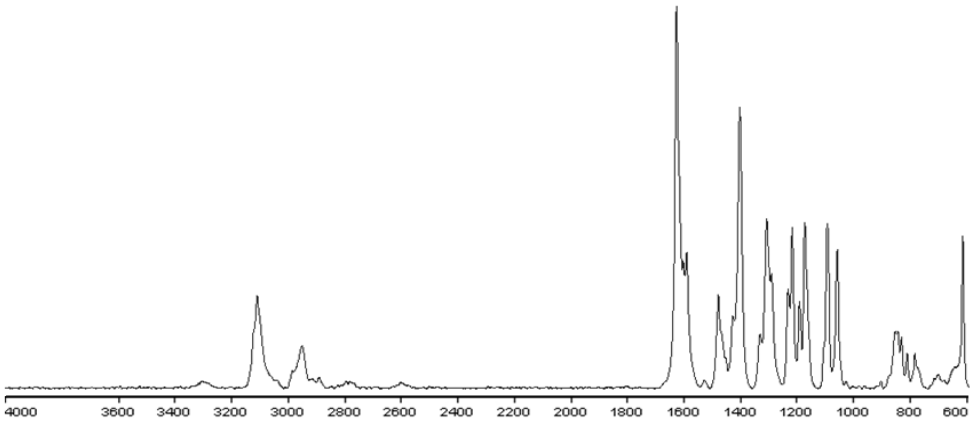

c) Raman spectrum of **NaTA·0.5 H_2O**.

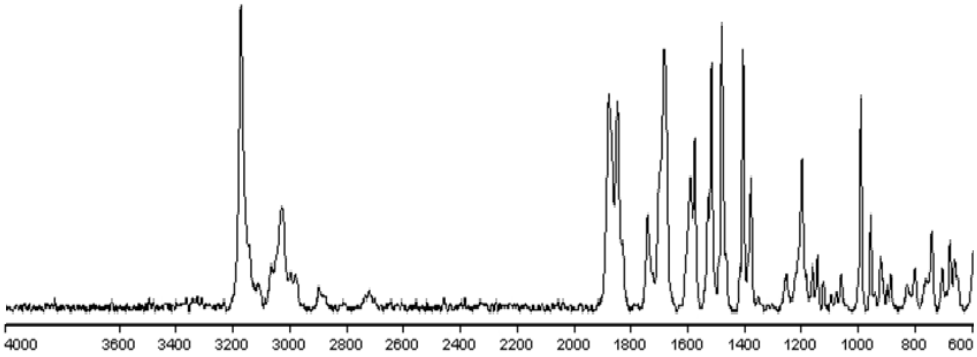

d) Raman spectrum of **NaTA HT Form**

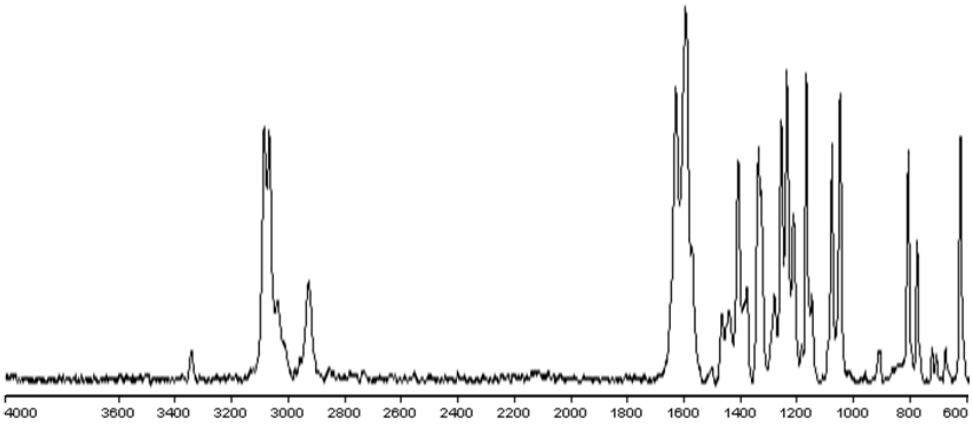

e) Raman spectrum of **NaTA·HTA·H_2O/$NaHCO_3$**.

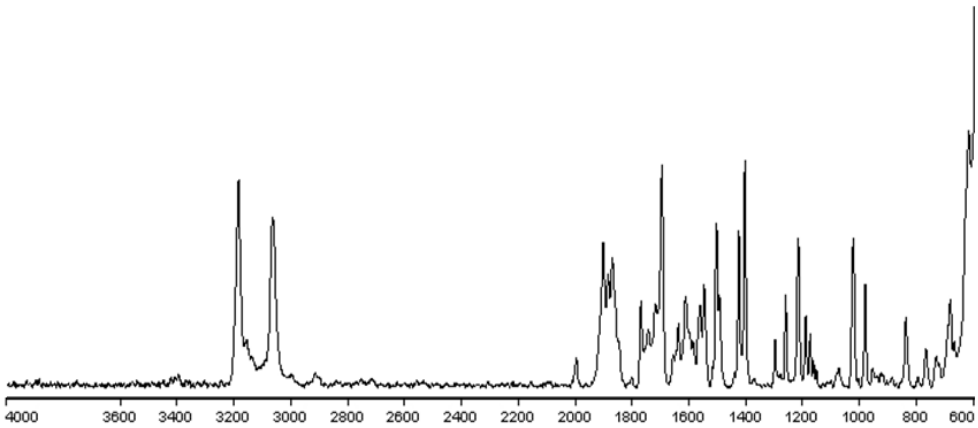

f) Raman spectrum of **NaTA·HTA·0.5NaAc·2H_2O**.

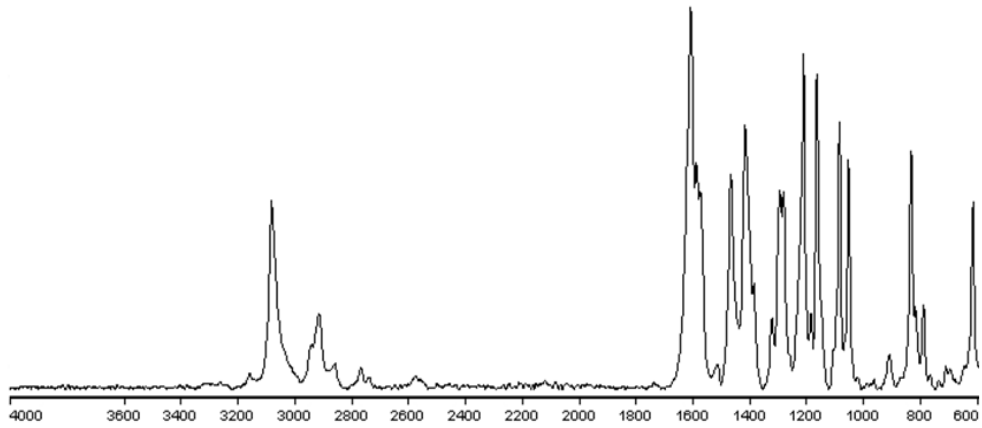

g) Raman spectrum of **IMH-TA·HTA**.

Figures S2: IR-ATR spectra of all prepared compounds

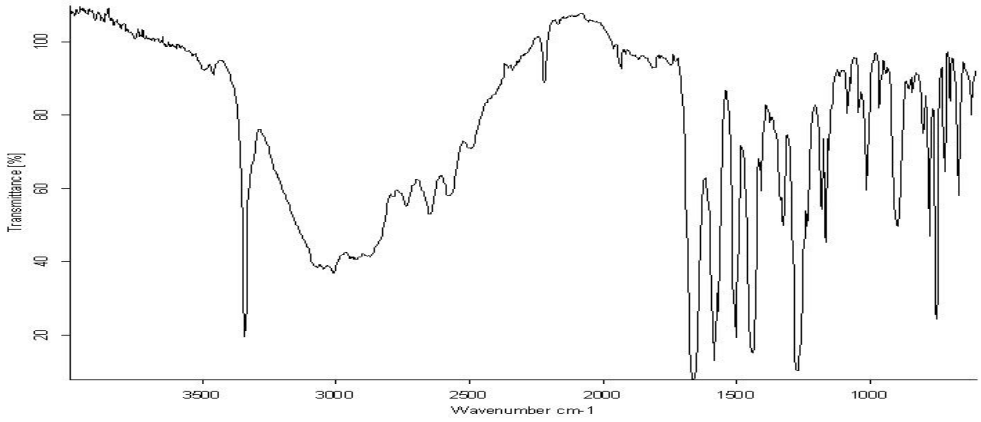

a) IR (KBr) spectrum of **HTA Form I.**

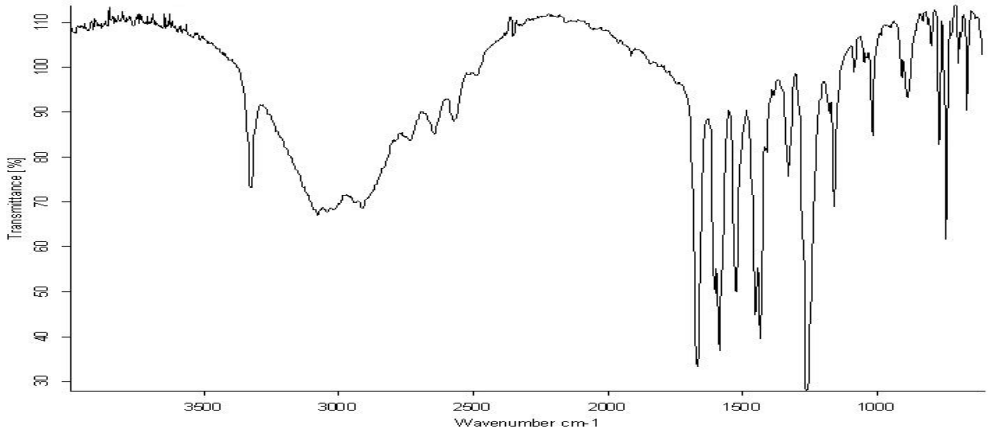

b) IR (KBr) spectrum of **HTA Form II**.

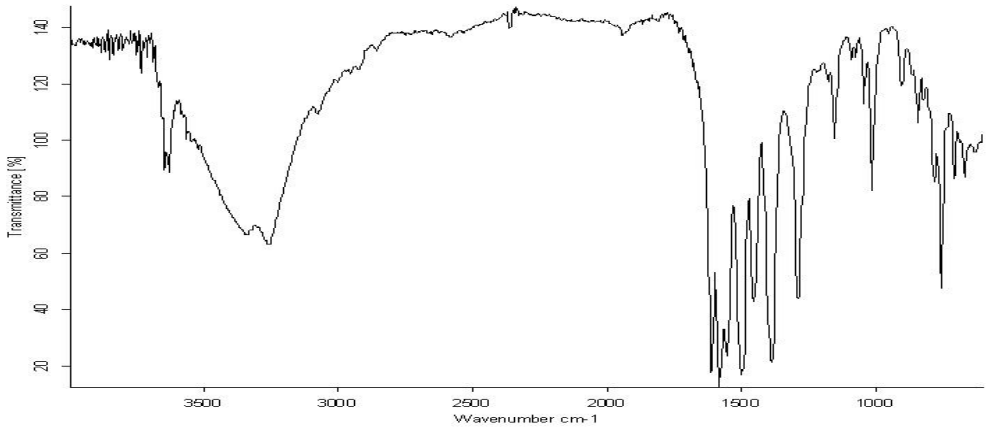

c) IR (KBr) spectrum of **NaTA·0.5H_2O**.

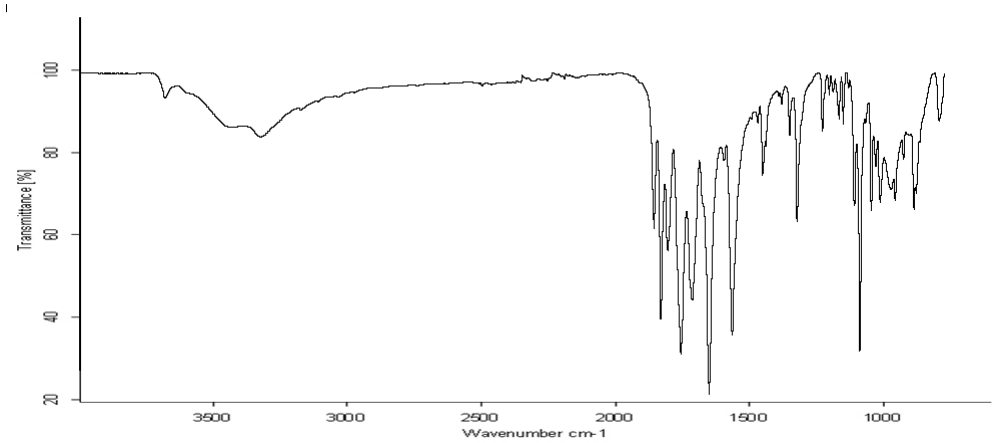

d) IR (ATR) spectrum of **NaTA HT Form**.

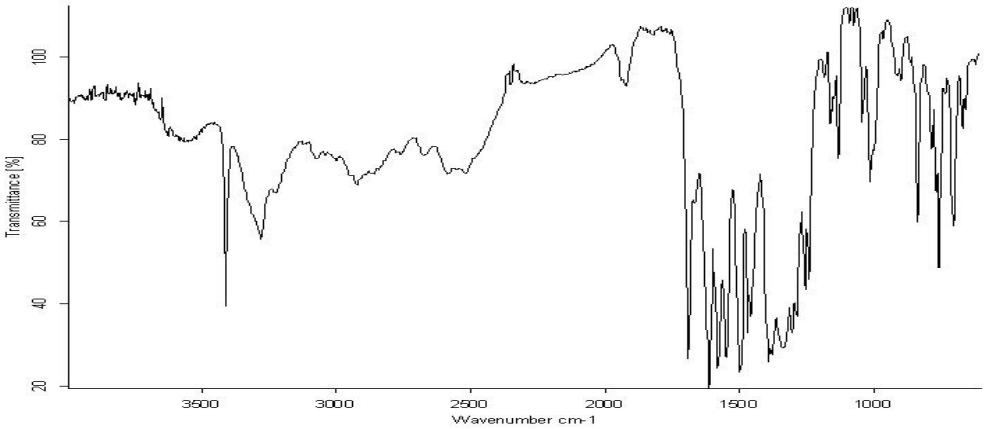

e) IR (KBr) spectrum of **NaTA·HTA·H_2O/$NaHCO_3$**.

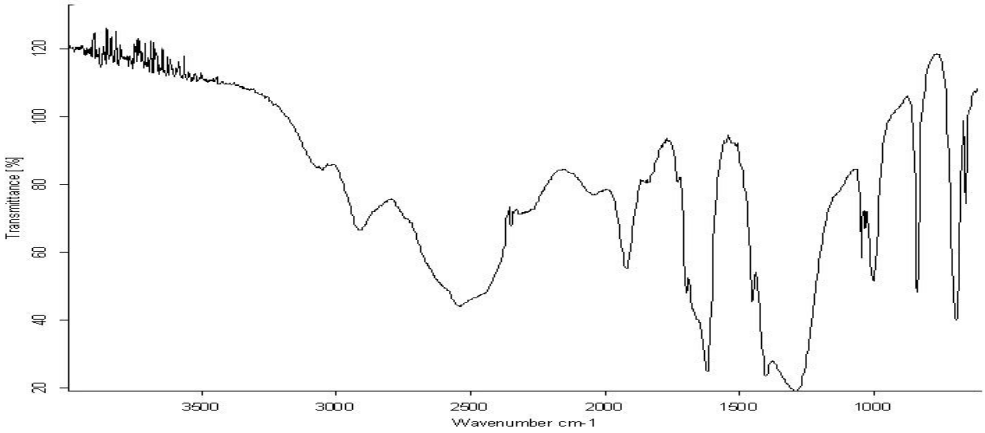

f) IR (KBr) spectrum of $NaHCO_3$.

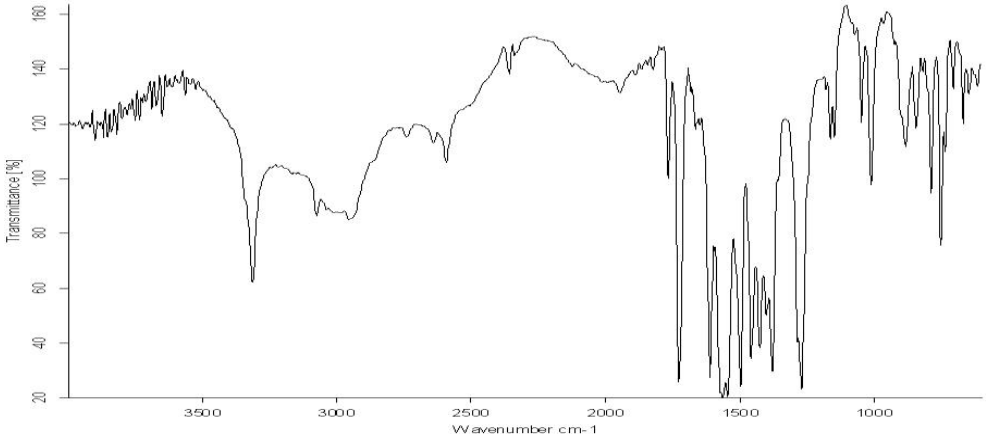

g) IR (KBr) spectrum of **NaTA·HTA·0.5NaAc·2H_2O**.

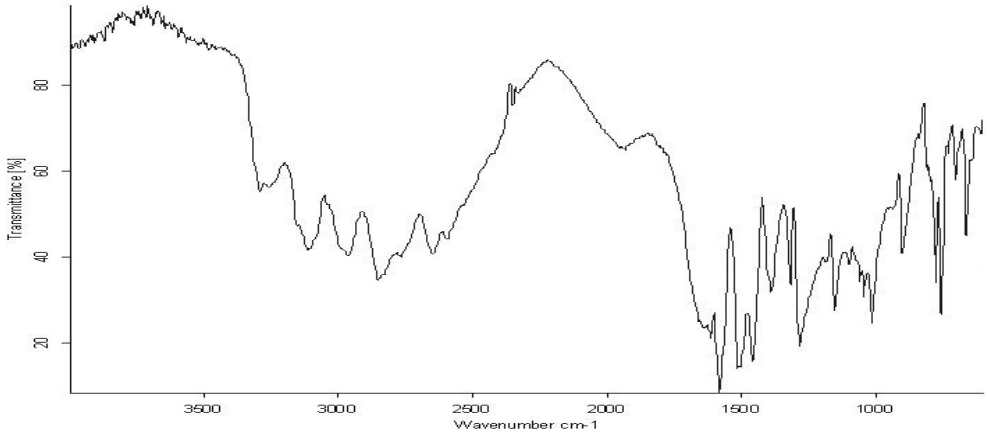

h) IR (KBr) spectrum of **IMH-TA·HTA**.

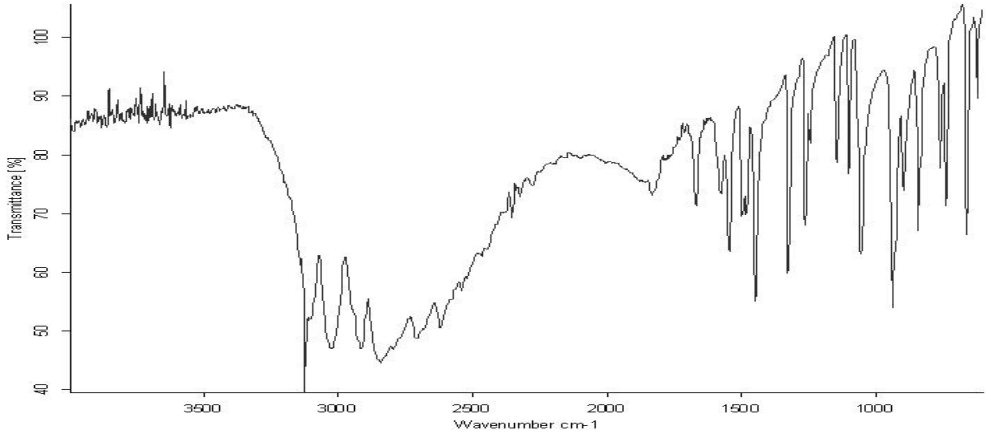

i) IR (KBr) spectrum of Imidazole (IM).

Figures S3: Calorimetric and Thermogravimetric curves of all compounds

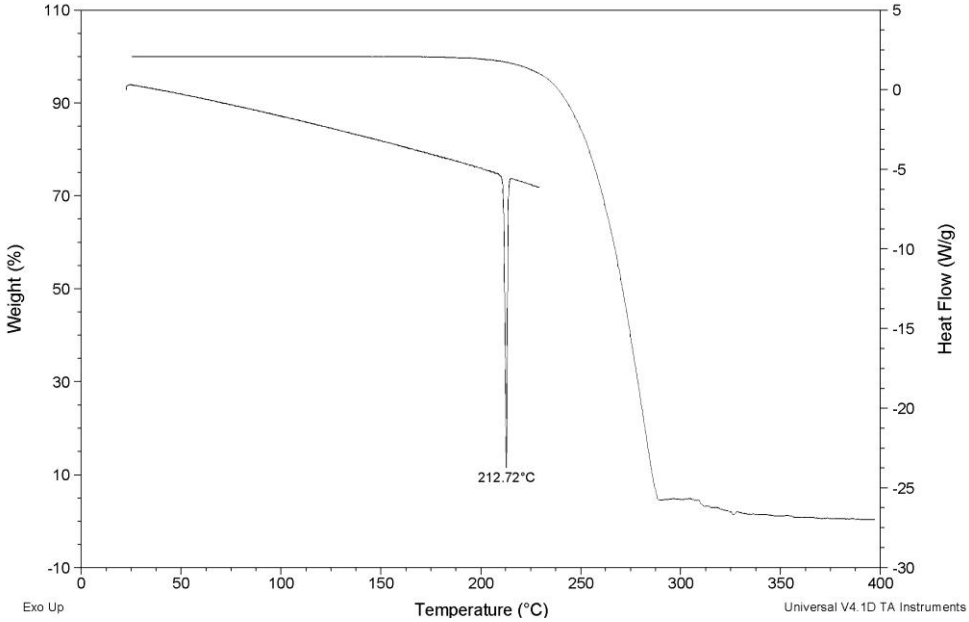

a) DSC and TGA curves of HTA Form I (batch)

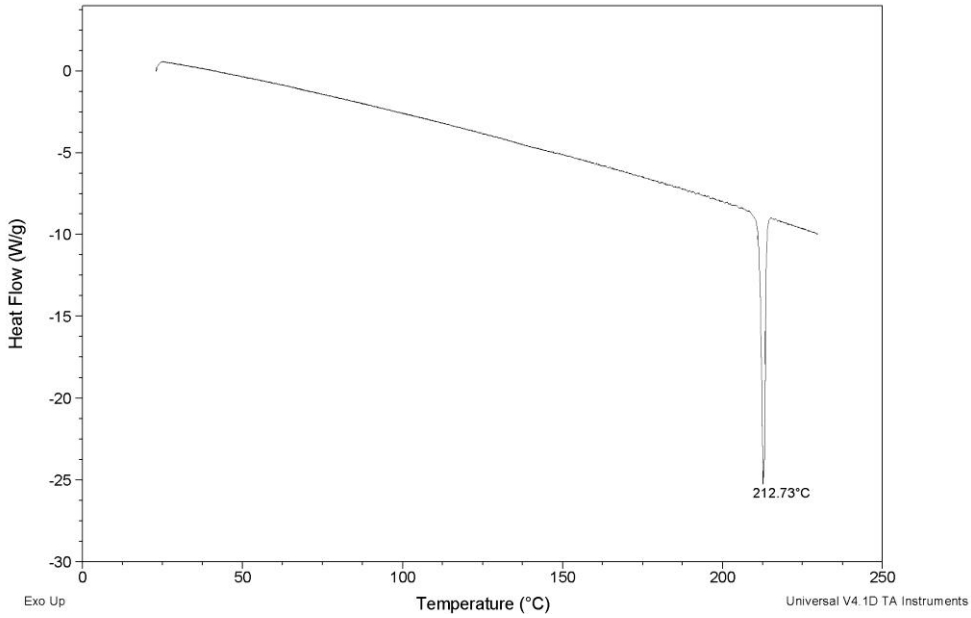

b) DSC curve of HTA Form II (the **Form I → Form II** conversion reported in literature was not observed)

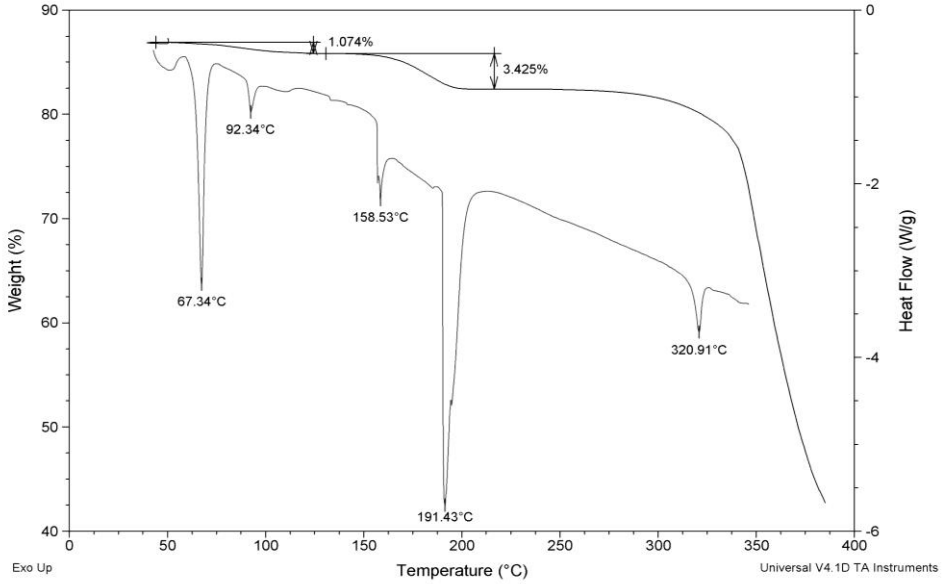

c) DSC and TGA curves of **NaTA·0.5H_2O.**The TGA curve of **NaTA·0.5H_2O** shows two steps attributed to adsorbed and stoichiometric H_2O loss, respectively. The DSC is quite complex since presents solid-solid transitions at 67.3 and 92.3°C leading to polymorphic mixtures as observed by ^{13}C CPMAS measurements (Figure S9) acquired on heated samples. On the other hand, the peak at 191.4 is assigned to the formation of **NaTA HT Form**.

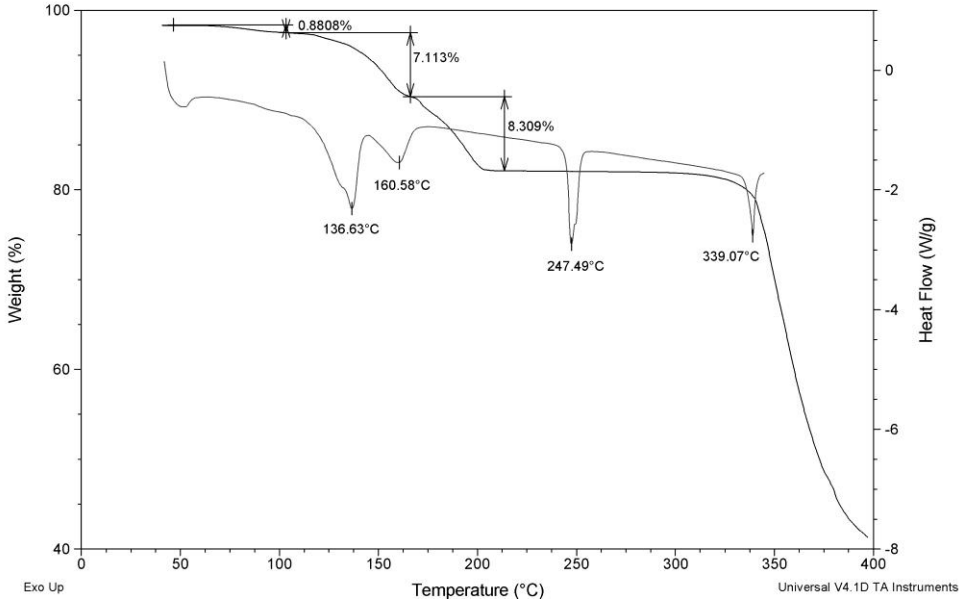

d) DSC and TGA curves of **NaTA·HTA·H_2O/$NaHCO_3$.** The two steps observed in the TGA curve are assigned to the release of CO_2 and H_2O, respectively. The high temperature regions (above 200°C) of TGA and DSC

of **NaTA·HTA·H_2O/$NaHCO_3$** is different from those of **NaTA·0.5H_2O** even if they both lead to **HTA HT Form** (as confirmed by ^{13}C CPMAS spectra). This is probably due to the different heating methods used or to the presence of small amount of impurities.

.

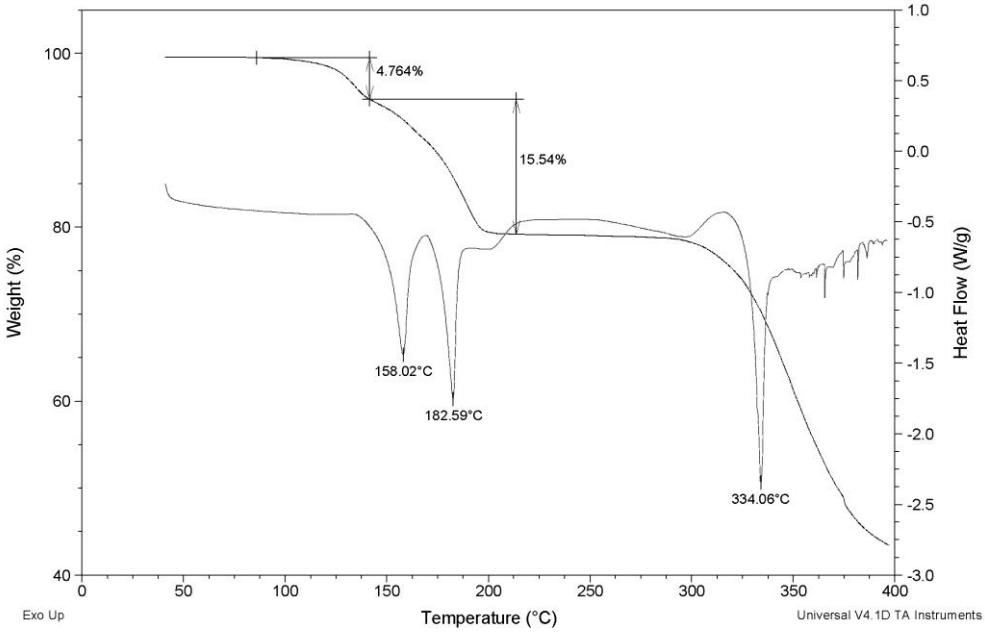

e) DSC and TGA curves of **NaTA·HTA·0.5NaAc·2H_2O**.

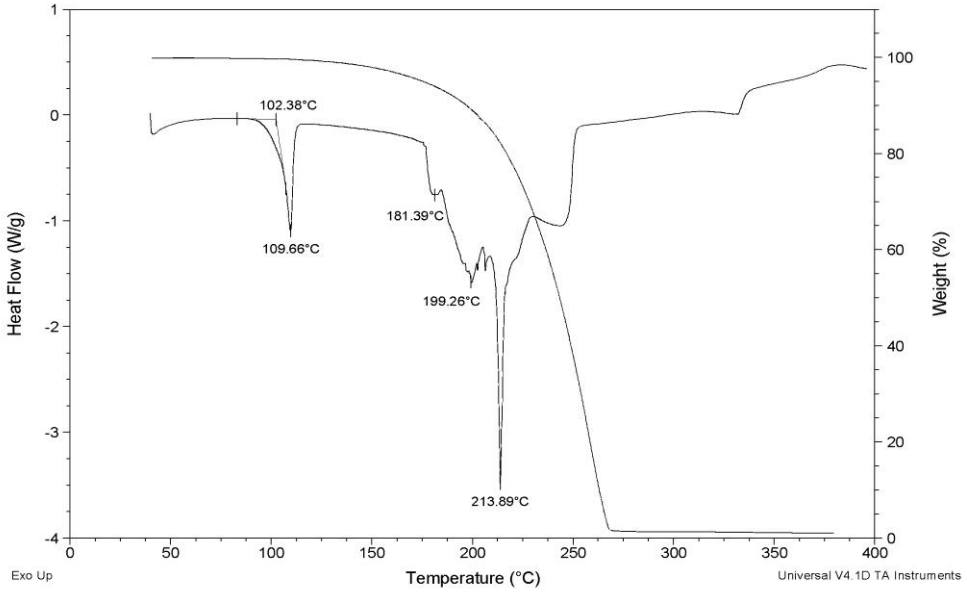

f) DSC and TGA curves of **IMH-TA·HTA**.

Figures S4: XRPD patterns of co-formers of HTA.

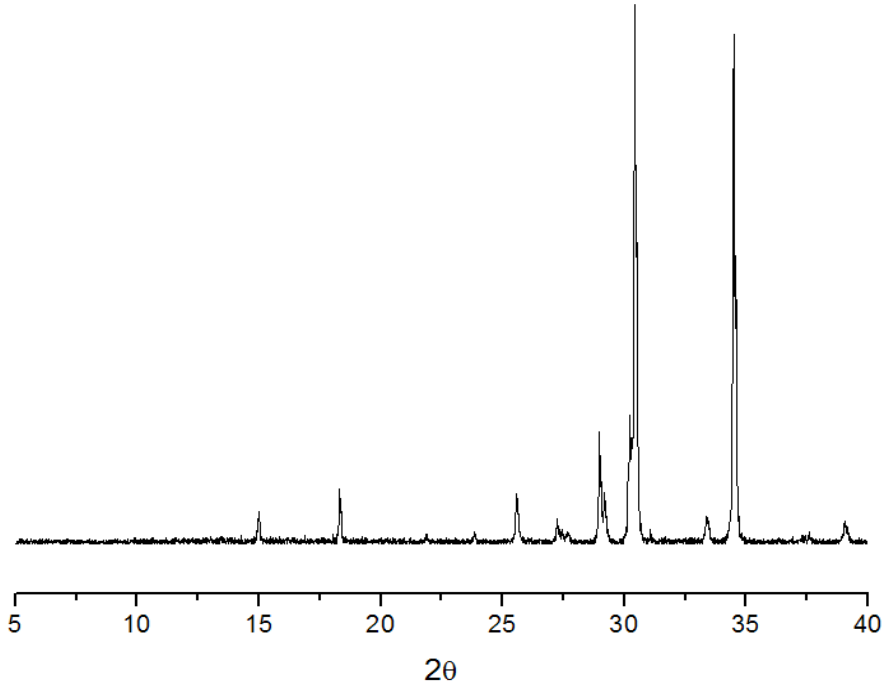

a) Experimental pattern of $NaHCO_3$.

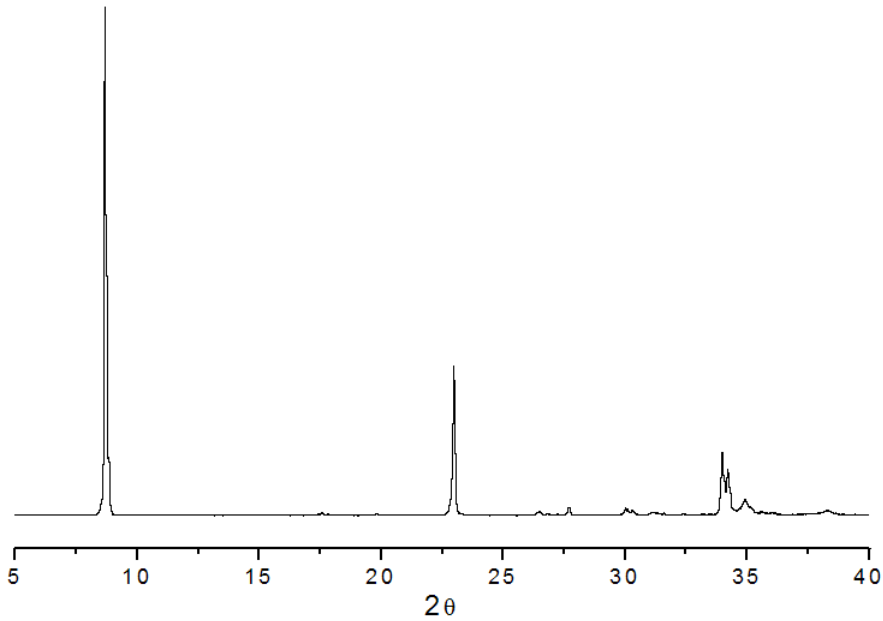

b) Experimental pattern of Sodium Acetate (NaAc).

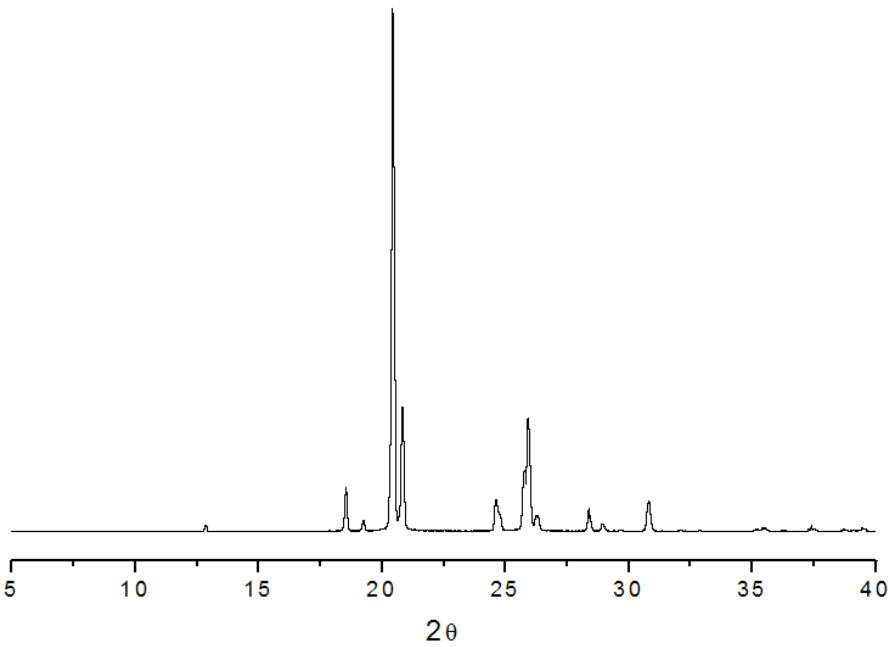

c) Experimental pattern of imidazole (IM).

Scheme 1: Temperature ramp applied to **NaTA·0.5 H_2O**

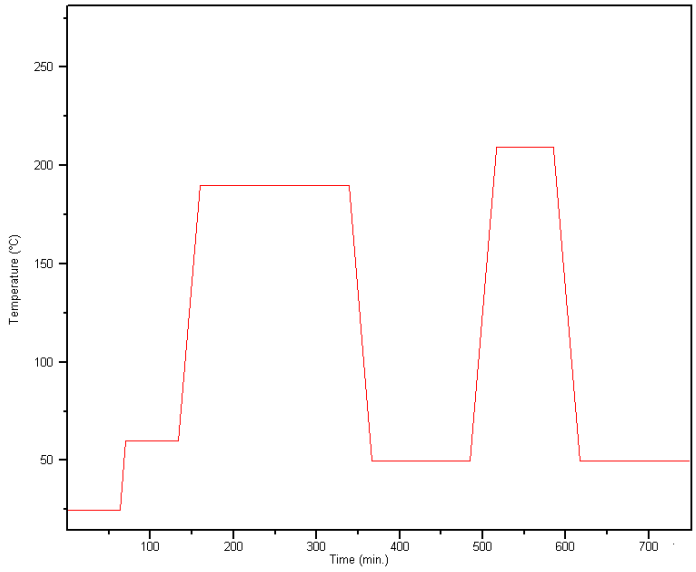

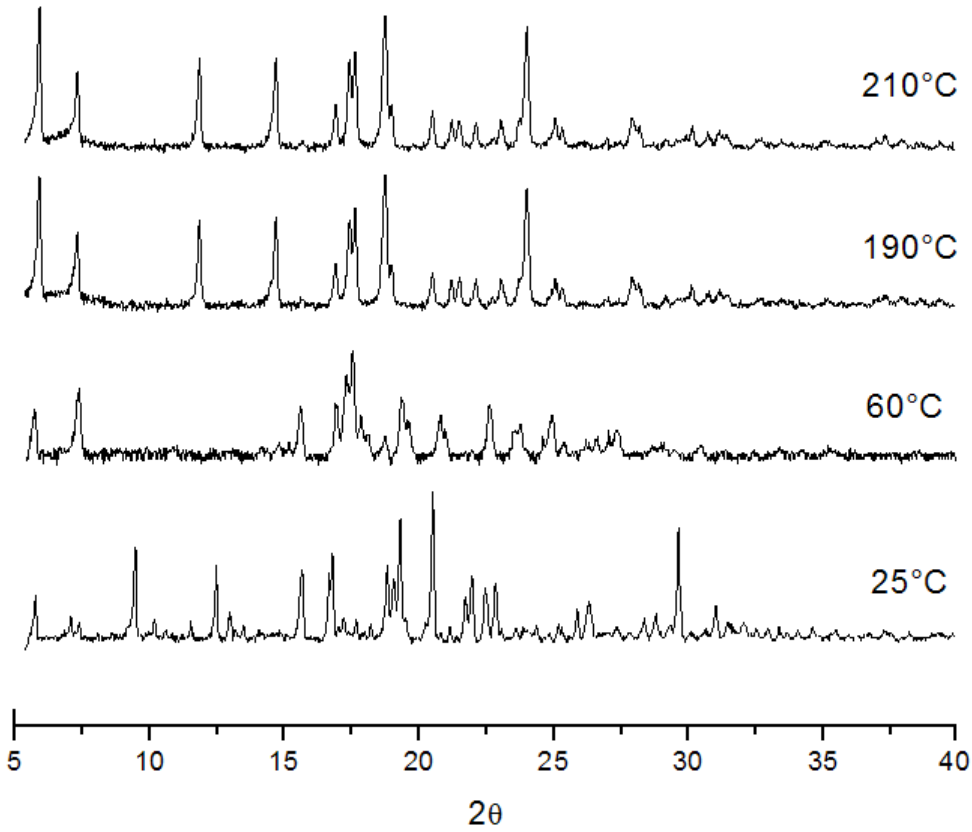

k) VT XRPD patterns of **NaTA·0.5 H_2O** from 25°C (r.t.) to 210 °C.

Scheme 2: Temperature ramp applied to **NaTA·HTA·H_2O/$NaHCO_3$**

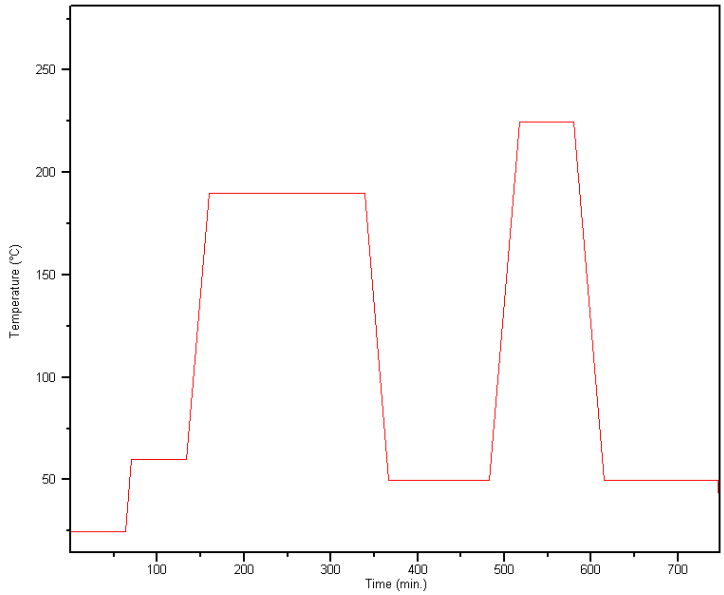

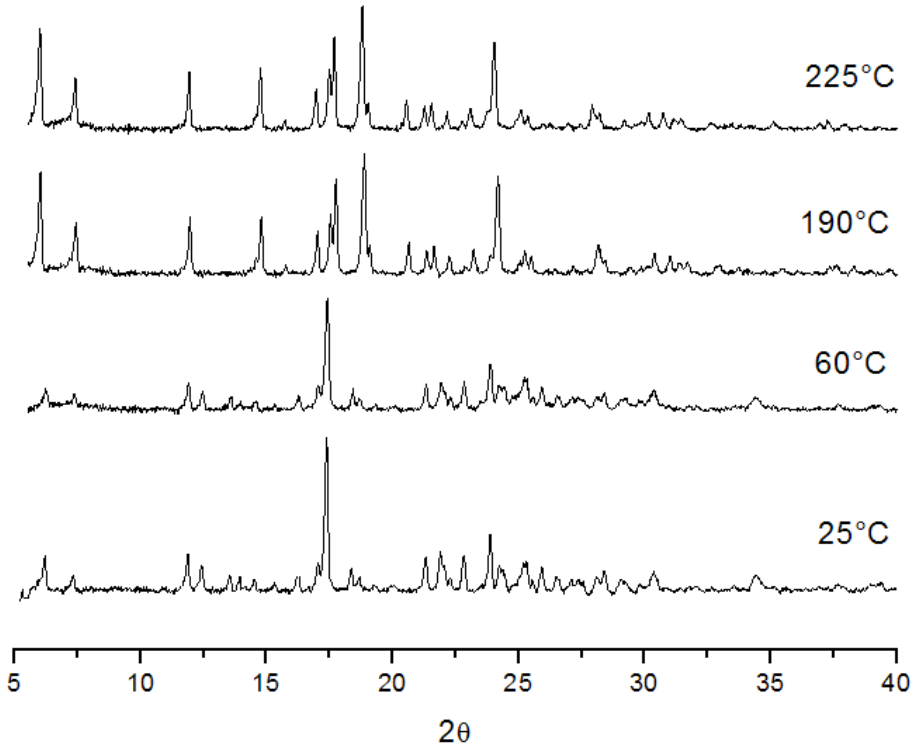

l) VT XRPD patterns of **NaTA·HTA·H_2O/$NaHCO_3$** from r.t. (25°C) to 225 °C.

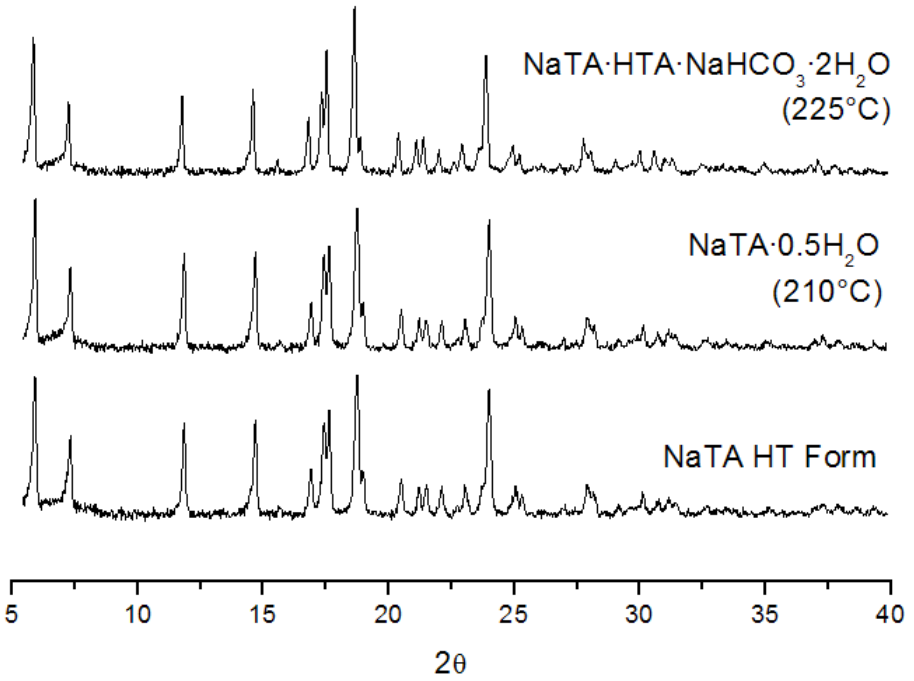

m) XRPD comparison between NaTA·HTA·H_2O/$NaHCO_3$ (after heating at 225°C), NaTA·0.5 H_2O (after heating at 210°C) and NaTA HT Form

A Variable Temperature (VT) XRPD study was performed and reported in Figures S3-c and S3-d for **NaTA·0.5 H_2O** and **NaTA·HTA·H_2O/$NaHCO_3$**, respectively). The ramp programs (Schemes 1 and 2) were set according to the most significant thermal transitions observed in the DSC and TGA data. The temperature was alternatively increased and decreased in order to check the irreversibility of the conversion processes. The VT XRPD analysis confirms the conversion of both **NaTA·0.5 H_2O** and **NaTA HTA H_2O/$NaHCO_3$** into the same **NaTA HT Form**, in agreement with the solid-state NMR and RAMAN characterization.

Figures S5: Dissolution kinetic tests (DKT)

Table 1: Standard solutions of pure HTA for the calibration curve

Solution	Conc (mg/l)	ABS
1	4.00E-01	1.68E+00
2	1.00E-01	4.63E-01
3	1.00E-00	6.49E-02
4	1.00E-01	2.01E-02
5	1.00E-02	1.25E-02
6	1.00E-03	2.08E-02

UV absorption spectrum of Solution 2.

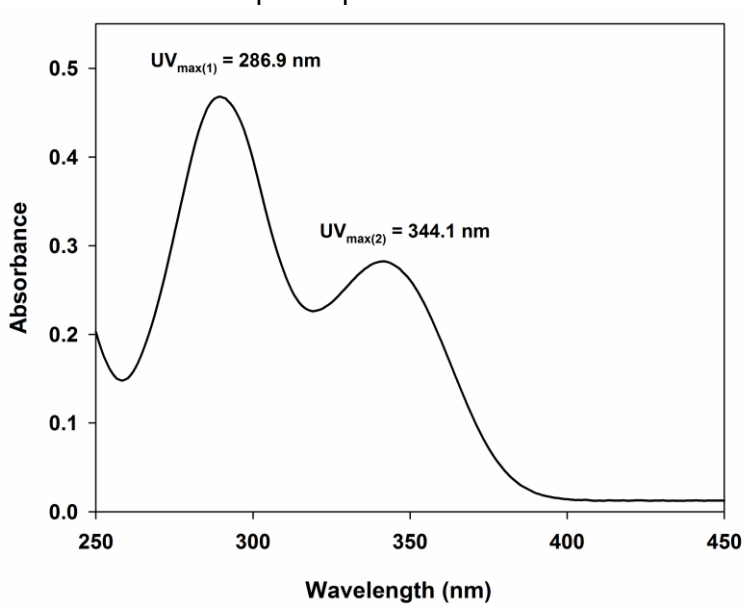

Calibration Curve of HTA at 286.9 nm

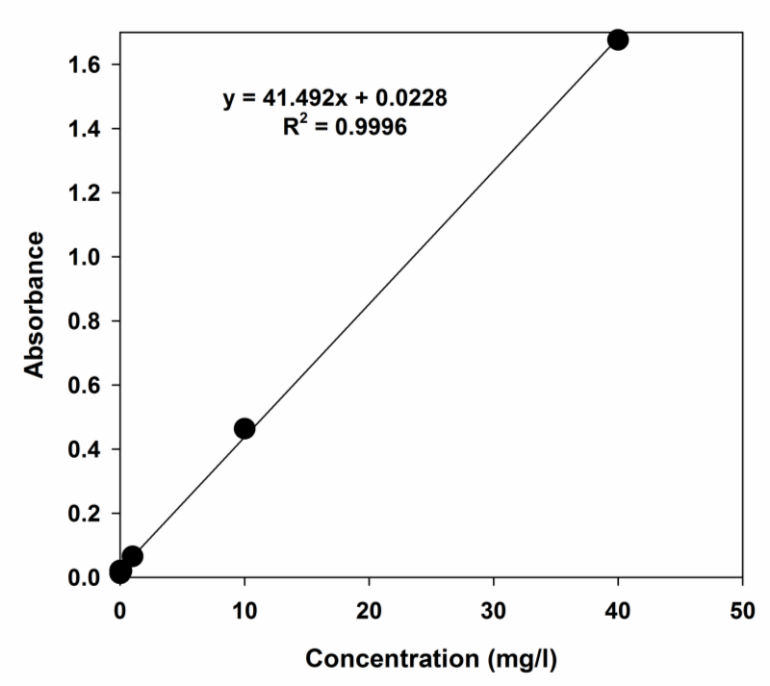
y = 41.492x + 0.0228
R2 = 0.9996
Absorbance
Concentration (mg/l)
0.0
0.2
0.4
0.6
0.8
1.0
1.2
1.4
1.6
0
10
20
30
40
50

Figure S6: ^{13}C CP MAS of **NaTA polymorphs mixture**. **^{13}C CPMAS** spectrum of **NaTA polymorphic mixture** obtained from HTA salification with NaOH; multiplicity and bandwidth of the signals highlight the co-presence of different polymorphic forms of NaTA.

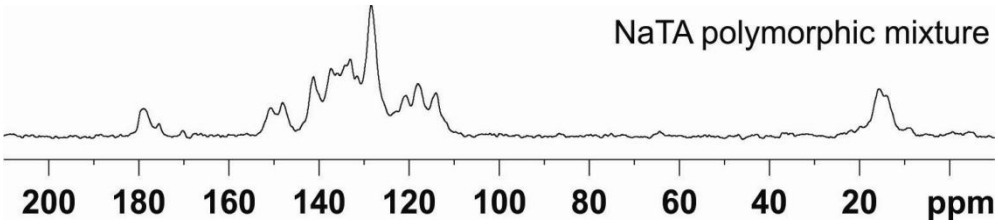

Figure S7: 2D ^{1}H-^{13}C FSLG on-resonance HETCOR spectrum of **NaTA·HTA·0.5NaAc·2H_2O**. 2D experiment acquired with a short contact times (100 µs) for highlighting only the short- (single bond) spatial proximities.

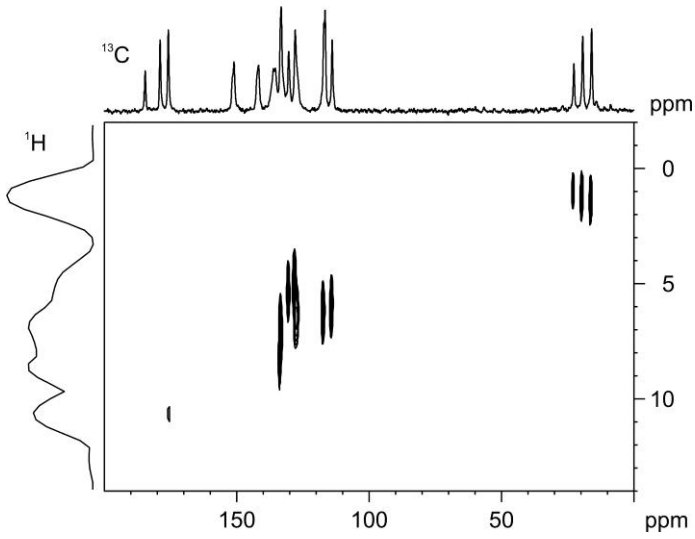

Figure S8: ^{13}C CPMAS of **NaTA·HTA·0.5NaAc·2H$_2$O** after thermal treatment. ^{13}C (100 MHz) CPMAS spectra of a) sodium acetate (batch of Sigma Aldrich), b) **NaTA·HTA·0.5NaAc·2H$_2$O**, c) **NaTA·HTA·0.5NaAc·2H$_2$O** heated at 150°C and d) **NaTA·HTA·0.5NaAc·2H$_2$O** heated at 250°C recorded at 12 kHz.

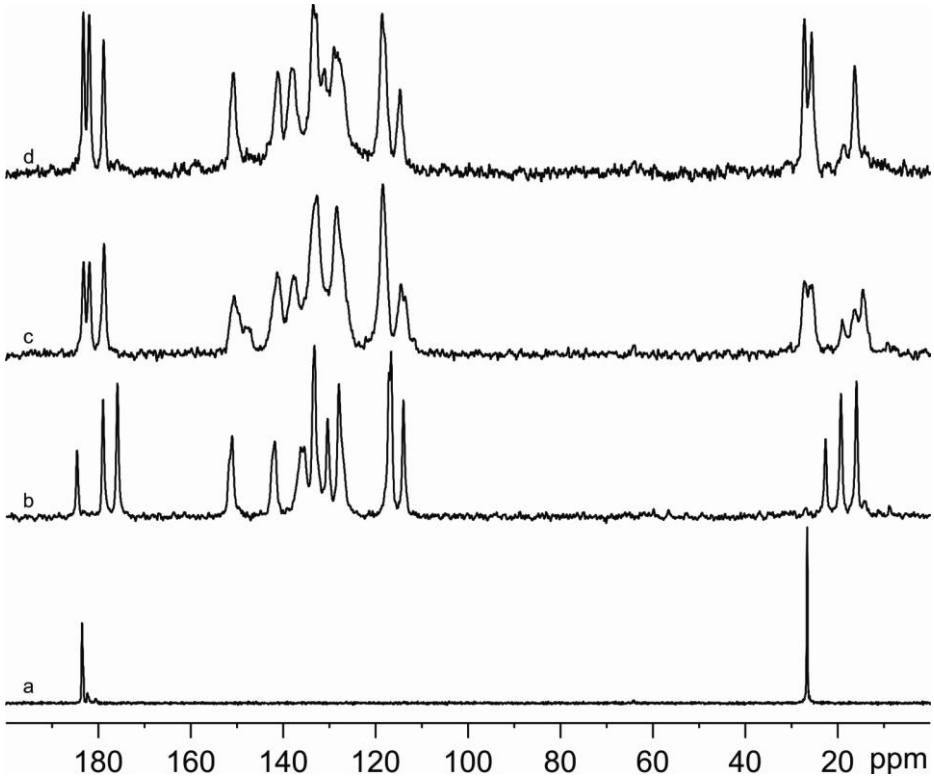

Figure S9: Dissolution rate profiles of the samples. **HTA** (red line with red circle), **NaTA·0.5H_2O** (blue line with blue square), **NaTA HT Form** (black line with yellow circle), **IMH-TA·HTA** (green line with green triangle), **NaTA·HTA·H_2O/Na_2CO_3·** (black line with black triangle) and **NaTA·HTA·0.5NaAc·2H_2O** (black line with white circle respectively)